LA-UR-03-4264

Approved for public release;
distribution is unlimited.

Title: Implementation of MARS Hadron Production and Coulomb Scattering Modules into LAHET

Author(s): N. V. Mokhov and S. I. Striganov,
Fermi National Accelerator Laboratory

Submitted to: for project distribution

Implementation of MARS Hadron Production and Coulomb Scattering Modules into LAHET

N. V. Mokhov and S. I. Striganov
Fermi National Accelerator Laboratory [1]

October 25, 2002

[1]This report documents work completed in a collaboration funded through Los Alamos National Laboratory, Diagnostic Applications Group X-5, under P.O. #39587.

Contents

Chapter 1

Introduction

The LAHET code system is widely used for simulation of particle transport and interactions. LAHET provides a possibility to use several generators for hadron-nucleus interaction at medium energies (Bertini model, ISABEL, Cugnon model), with the FLUKA model available at high energy. The inclusive generator of hadron-nucleus interactions of the MARS14 code [1] is based on experimental data and described in [2],[3]. Use of an inclusive approach can provide higher computing efficiency compared to analog calculations.

Multiple Coulomb scattering in LAHET is simulated by means of Rossi distribution [4]. It is known that this approach is not accurate for small and medium track lengths [6],[7]. A newly developed MARS algorithm provides precise and efficient description of angular deflection due to multiple Coulomb scattering for an arbitrary step size.

This report gives a short description of the above MARS physical modules and their implementation into LAHET.

Chapter 2

Inclusive Event Generator

2.1 Inclusive and exclusive approaches in simulation of hadronic cascades

First, let's consider a simplified model of a hadronic cascade - a cascade of identical particles. A probability $P(S, E_0, x)$ to get a signal S due to interactions of a particle of energy E_0 with a block of matter of thickness x can be written as

$$P(S,E_0,x) = \int_0^{E_0} dE f_c(E_0,E,x) P_c(S,E_0,E,x) e^{-\Sigma_d x} +$$

$$\int_0^x dx_0 \Sigma_d e^{-\Sigma_d x_0} \int_0^{E_0} dE f_c(E_0,E,x_0) \sum_{n=1}^{n_{max}} \int \prod_{i=1}^{n} d\varepsilon_i W(E,n,\varepsilon_1,...,\varepsilon_n)$$

$$\int_0^{\infty} dS_0 \Big[\prod_{i=1}^{n} dS_i P(S_i,\varepsilon_i,x-x_0) \Big] P_c(S_0,E_0,E,x_0) \delta(S - \sum_{i=0}^{n} S_i), \qquad (2.1)$$

where $f_c(E_0, E, x)$ is a probability to lose energy $E_0 - E$ on a length x in "continuous" collisions; $P_c(S, E_0, E, x)$ is a probability to get signal S in such collisions; $W(E, n, \varepsilon_1, ..., \varepsilon_n)$ is a probability to create n particles with energies $\varepsilon_1, ..., \varepsilon_n$ in a discrete interaction at energy E.

The average signal of such a cascade is then

$$\bar{S}(E_0,x) = \int_0^{\infty} dS S P(S,E_0,x) \int_0^{E_0} dE f_c(E_0,E,x) \bar{S}_c(E_0,E,x) e^{-\Sigma_d x} + \int_0^x dx_0 \Sigma_d e^{-\Sigma_d x_0}$$

$$\int_0^{E_0} dE f_c(E_0,E,x_0) \{ \bar{S}_c(E_0,E,x_0) + \int_0^E d\varepsilon H(E,\varepsilon) \bar{S}(\varepsilon, x-x_0) \}, \qquad (2.2)$$

where

$$\bar{S}_c(E_0, E, x) = \int_0^\infty dSSP_c(S, E_0, E, x),$$

and

$$H(E, \varepsilon) = \sum_{n=1}^{n_{max}} n \int d\varepsilon_2 ... d\varepsilon_n W(E, n, \varepsilon, \varepsilon_2, ..., \varepsilon_n)$$

is a single-particle inclusive spectrum. Note, that such differential cross sections are usually measured in experiments.

To calculate the average signal of a cascade, one can use the following probability distribution

$$\tilde{P}(S, E_0, x) = \int_0^{E_0} dE f_c(E_0, E, x)\delta[S - \bar{S}_c(E_0, E, x)]e^{-\Sigma_d x}$$

$$+ \int_0^x dx_0 \Sigma_d e^{-\Sigma_d x_0} \int_0^{E_o} dE f_c(E_0, E, x_0) \int_0^E d\varepsilon \varphi(E, \varepsilon) \int dS_1 dS_2$$

$$\delta(S - S_1 - WS_2)\delta[S_i - \bar{S}_c(E_0, E, x_0)]\tilde{P}(S_2, \varepsilon, x - x_0), \qquad (2.3)$$

where $\varphi(E, \varepsilon)$ is an arbitrary normalized probability distribution and a weight W is defined as

$$W = H(E, \varepsilon)/\varphi(E, \varepsilon).$$

Note, that the average signal which is obtained using distribution (2.3) coincides with the average value (2.2) of distribution (2.1). Expression (2.3) gives a recipe to calculate an average signal of hadronic cascades using information on inclusive spectra only. The same results can be obtained for a three-dimensional cascade with several types of particles.

To estimate efficiency of an inclusive method one should consider further simplified model of a cascade: a cross section (Σ) does not depend on energy and a mean multiplicity of secondary particles in any interaction is equal to $\bar{n}$ independent of the initial energy. Such a model could provide a crude estimation of an initial stage of a cascade. Using above formulae (2.1) - (2.3), one can calculate the average number of particles and its variance at a depth x using the exclusive method

$$N_{ex} = e^{\Sigma x(\bar{n}-1)}$$

and

$$D^2_{ex} = \overline{N^2}_{ex} - \overline{N}^2_{ex} = \frac{\overline{(n-1)^2}}{\overline{n}-1}(\overline{N}^2_{ex} - \overline{N}_{ex})$$

In the exclusive method one simulates

$$V_{ex} = e^{\Sigma x(\bar{n}-1)}/(\bar{n}-1)$$

interactions.

In an inclusive approach, one simulates a smaller number of interactions, $V_{inc} = \Sigma x$. The average number of particles at a depth x calculated by means of the inclusive method is the same as for the exclusive one: $N_{inc} = e^{\Sigma x(\bar{n}-1)}$. But the variance is larger

$$D^2_{inc} = e^{\Sigma x(\bar{n}^2-1)} - e^{2\Sigma x(\bar{n}-1)}.$$

An efficiency of the method is inversely proportional to CPU time needed to obtain a variance D

$$\varepsilon \sim \frac{1}{D^2 V \tau}, \tag{2.4}$$

where V is the average number of interactions, τ is a CPU time to simulate one interaction.

A relative efficiency of exclusive and inclusive methods can be written as

$$\frac{\varepsilon_{ex}}{\varepsilon_{inc}} = \frac{\Sigma x e^{\Sigma x(\bar{n}^2-3\bar{n}+2)}(1 - e^{-\Sigma x(\bar{n}-1)^2})\tau_{inc}}{r(1 - e^{-\Sigma x(\bar{n}-1)})^2 \tau_{ex}}, \tag{2.5}$$

where

$$r = \frac{\overline{(n-1)^2}}{\overline{(n-1)}^2}$$

One can increase efficiency of the inclusive method by using splitting. If one generates $\bar{n}$ secondary particles with a weight of one instead of one particle with the weight $\bar{n}$, then the ratio of efficiencies becomes simply

$$\frac{\varepsilon_{ex}}{\varepsilon_{inc}} \sim \frac{\tau_{inc}}{\tau_{ex}}.$$

Table 2.1 shows the CPU time needed to simulate a proton iron interaction by means of LAHET3.16 using FLUKA and MARS options. The inclusive MARS generator is a few times faster than the exclusive FLUKA. So, simulation of hadronic cascade using a smart inclusive approach can be more effective then an exclusive method.

Experimental data shows that about a half of primary hadron energy in a hadron nucleus interaction is transfered to one particle (so called, leading particle) and the other half is shared between a number of secondaries. To obtain a more realistic estimation of efficiencies of exclusive and inclusive methods, let's consider a simple model of hadron-nucleus interactions which takes into account the leading particle effect. The number of secondary particles in a hadron-nucleus interaction is generated from a Poisson distribution with an average multiplicity $N(E)$ taken from experimental data. Energy of a leading hadron is generated from a uniform distribution with mean value equal to a half of the primary hadron energy; remaining energy is equally shared between the other particles. One can apply such a model to simulate hadronic cascade

Table 2.1: Relative CPU per event in LAHET for FLUKA (ex) and MARS (inc) models

E, GeV	5	10	25	50	100
τ_{ex}/τ_{inc}	3.1	3.2	4.9	5.5	5.7

using different methods - exclusive (analog), inclusive or leading particle bias (LPB) approaches. In the LPB method, one simulates two secondary particles in each vertex: a leading hadron with the weight of unity and one of the other secondaries with the weight of $N(E) - 1$. Longitudinal distributions of hadron flux ($E > 50$ MeV) in an iron-concrete block irradiated by a 50 GeV proton calculated with exclusive (analog) and LPB methods are shown on Fig. 2.1. The fluxes coincide within statistical errors, but efficiency of the LPB approach is substantially higher up to a thickness of 160 cm.

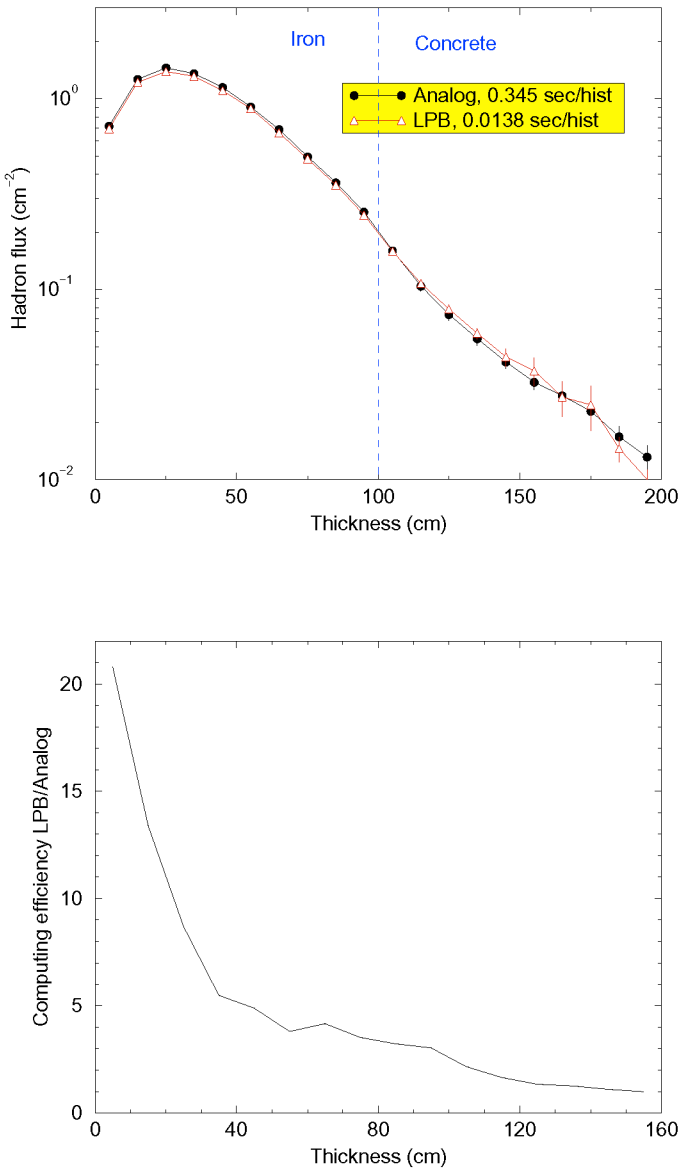

Figure 2.1: Hadron flux in an iron+concrete block irradiated with 50 GeV protons.

2.2 Phenomenological model of hadron nucleus collisions

To simulate hadronic cascades using an inclusive approach, one needs - among other things - total cross sections and inclusive spectra. In MARS, total cross sections at energies above 5 GeV are calculated by means of the Glauber model with inelastic corrections [2]. Comparison of MARS calculations and experimental data is shown in Figs. 2.2 - 2.4.

Hadron double differential cross sections in MARS are described in the form

$$\frac{d^2\sigma^{h_1A\to h_2X}}{dpd\Omega} = R^{h_1A\to h_2X}(A, E_0, p, p_\perp)\frac{d^2\sigma^{h_1p\to h_2X}}{dpd\Omega}, \tag{2.6}$$

where p and $p_\perp$ are the total and transverse momenta of secondary hadron h_2, E_0 is the energy of primary hadron h_1 and A is the atomic mass of the target nucleus.

Comparison of the MARS description of proton-proton interactions is presented in Figs. 2.5 - 2.8. It is seen that the model reproduces the main features of pion and proton yields at least for energies below several hundred GeV.

The function $R^{h_1A\to h_2X}$, measured with much higher precision than the absolute yields, is almost independent of $p_\perp$ and its dependence on p_0 and p is much weaker than for the differential cross-section itself. Because of rather different properties of hadron production on nuclei in the forward (x_F >0) and backward (x_F <0) hemispheres, where x_F is the Feynman's longitudinal variable, we treat these two regions differently. Ratio $R^{h_1A\to h_2X}$ in the forward hemisphere was calculated for carbon, iron and tungsten at number of initial energies using the DPMJET2.4 code. The A-dependence of fast particle production for other nuclei and energies is obtained by interpolation. Experimental data on A-dependence for $x_F < 0$ is rather scarce. Stenlund and Otterlund have found a scaling for pseudo-rapidity distributions of shower particles (charged particles with $\beta > 0.7$) in proton-nucleus collisions at 20 – 400 GeV/c in the form

$$\frac{Y_0}{< N >}\cdot\frac{dN}{d\eta} = f(A, \frac{\eta}{Y_0}),$$

where $< N >$ is a mean multiplicity of shower particles, Y_0 is rapidity of primary proton and $\eta = -log(tan(\frac{\theta}{2}))$ is a pseudo-rapidity of a secondary particle. This approximation is in a reasonable agreement with data at energies above 7 GeV/c. An example of a such scaling behavior is shown in Figs. 2.9 - 2.10. The ratio of pseudo-rapidity distributions in hadron-nucleus and hadron-proton collisions is used for calculation of $R^{h_1A\to h_2X}$ at $x_F \leq 0$.

There is a lot of data on pion production in proton-nucleus collisions. For this channel, we use a model-independent approach [3]. The atomic mass dependence of differential cross sections is convenient to describe as A^α. A compilation of experimental

data on α for π^--production is shown in Fig. 2.11. For protons with energy ≥ 24 GeV and $p_\perp < 1GeV/c$, the A-dependence can be parameterized as

$$\alpha_g = 0.8 - 0.75 * x_F + .45 * x_F^3/|x_F| + 0.1 * p_\perp^2$$

For lower momenta, α is approximated as

$$\alpha = \alpha_g - 0.0087 \cdot (24 - p_0) \tag{2.7}$$

The $R^{pA\to\pi^\pm X} \sim A^\alpha$ form doesn't extrapolate well to A=1 because of the difference in the π-yield in proton-proton and proton-neutron collisions. This difference can be taken into account if one uses the following form for $R^{pA\to\pi^\pm X}$:

$$R^{pA\to\pi^\pm X} = (\frac{A}{2})^\alpha \cdot f(p_0, Y), \tag{2.8}$$

where $f(p_0, Y) = \frac{d\sigma}{dp}(pd \to \pi^\pm)/\frac{d\sigma}{dp}(pp \to \pi^\pm)$. It turns out that pion yields in pd and pp collisions are not very different, i. e. $f(p_0, Y) \approx 1$. Using FRITIOF results, we found that $f(p_0, Y)_{\pi^-} = 1 + 0.225/N_{\pi^-} - a_{\pi^-} \cdot Y_{cms}$, where N_{π^-} is a mean π^- multiplicity in pp-collisions and Y_{cms} is pion rapidity in the center-of-mass system (CMS). Data shows linear dependence of N_{π^-} on *free energy* $W = \frac{(\sqrt{s}-2\cdot m_p)^{0.75}}{\sqrt{s}^{0.25}}$, where $\sqrt{s}$ is the CMS collision energy. Our fit to the data gives $N_{\pi^-} = 0.81 \cdot (W - 0.6)$. The other parameter $a_{\pi^-} = 0.16$ for $p_0 \leq 20$ GeV/c, and depends on energy for higher momenta as $a_{\pi^-} = -0.055 + 0.747/log(s)$. $f(p_0, Y)_{\pi^-}$ is forced to be 1 if it becomes less than 1. For π^+ production the approximation is much simpler $f(p_0, Y)_{\pi^+} = 0.85 + 0.005 \cdot p_0$ for $p_0 \leq 30$ GeV/c and $f(p_0, Y)_{\pi^+} = 1$ for higher momenta.

A pseudo-rapidity is not a convenient variable for estimation of a very forward particle production. Shower particles are mixture of charged pions, kaons and protons. Yields of these particles have different dependencies on momentum. Therefore, one can obtain better description using rapidity. Experimental data on rapidity distribution of pion from proton nucleus collisions from 10 to 360 GeV/c is available. We have found that scaling in the form similar to Oterlund-Stenlund is valid

$$\frac{dN}{dY} = \frac{< N >}{Y_0} \cdot F(A, \frac{Y}{Y_0}), \tag{2.9}$$

where $< N >$ is a mean multiplicity of pions, Y_0 is a rapidity of primary proton and Y is a rapidity of pion (Figs. 2.12 - 2.13). Scaling function can be approximated as

$$F(A, \frac{Y}{Y_0}) = c_1 \cdot exp(-(\frac{Y}{Y_0} - c_2)^2/c_3),$$

Experimental data on rapidity distribution of π^+,π^- in proton-proton interaction can be fitted as

$$\frac{dN}{dY} = C_{pp} \cdot exp(-\frac{Y_{cm}^2}{2\sigma^2}), \tag{2.10}$$

where Y_{cm} is a pion rapidity in the center-of-mass system.

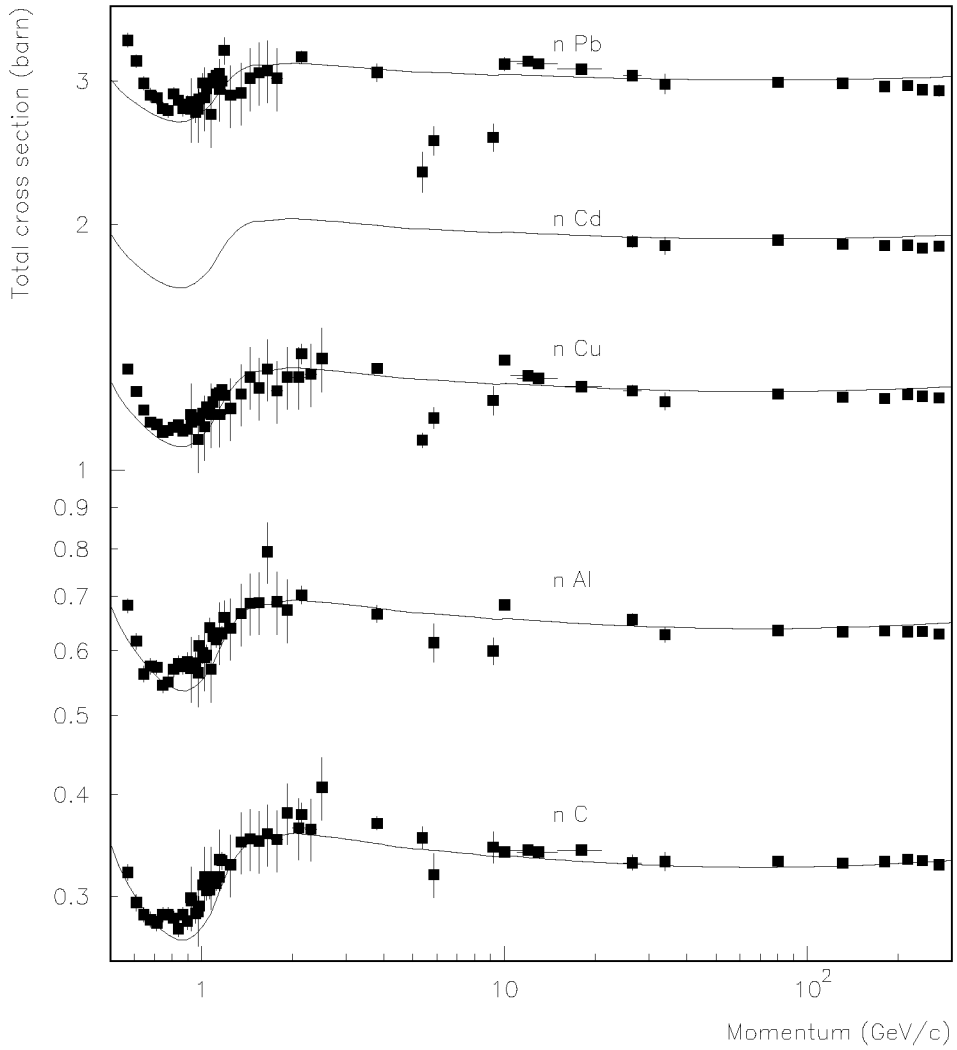

Figure 2.2: Neutron-nucleus total cross sections.

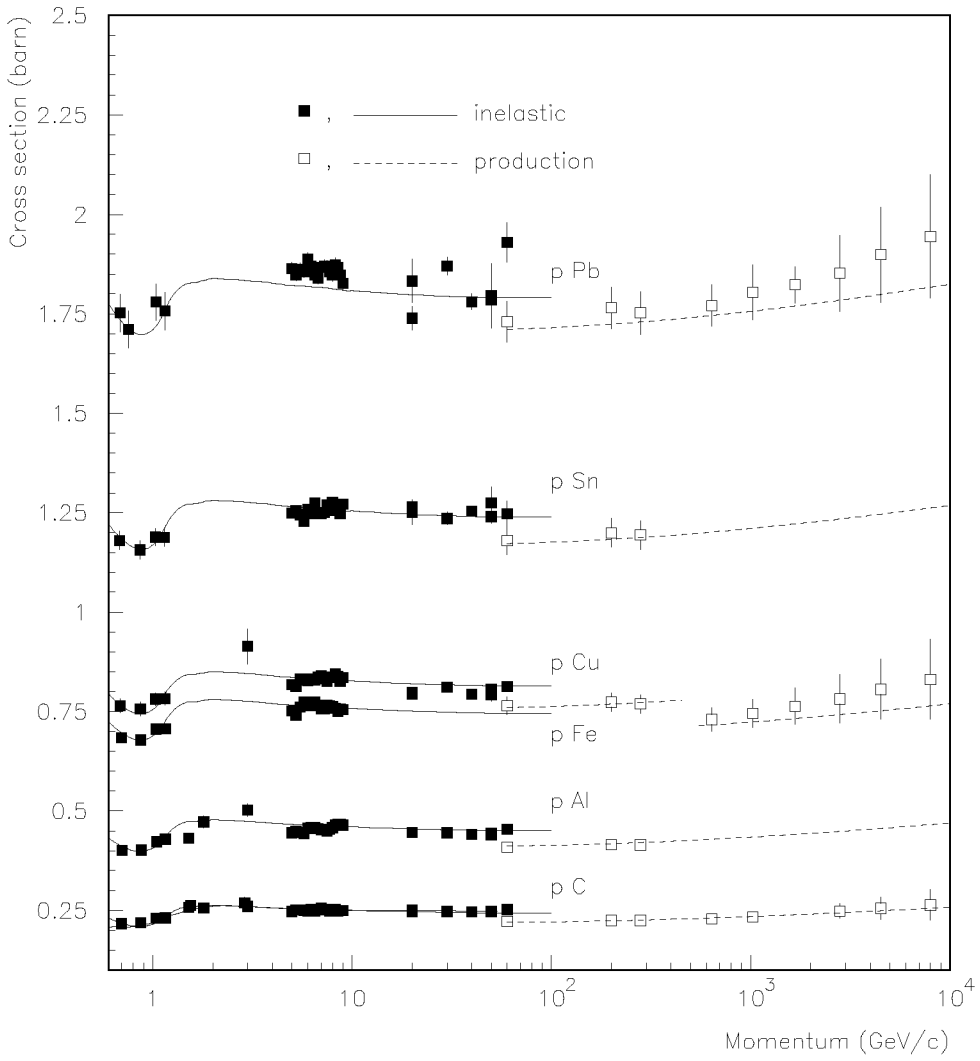

Figure 2.3: Inelastic and production cross sections of proton-nucleus interactions.

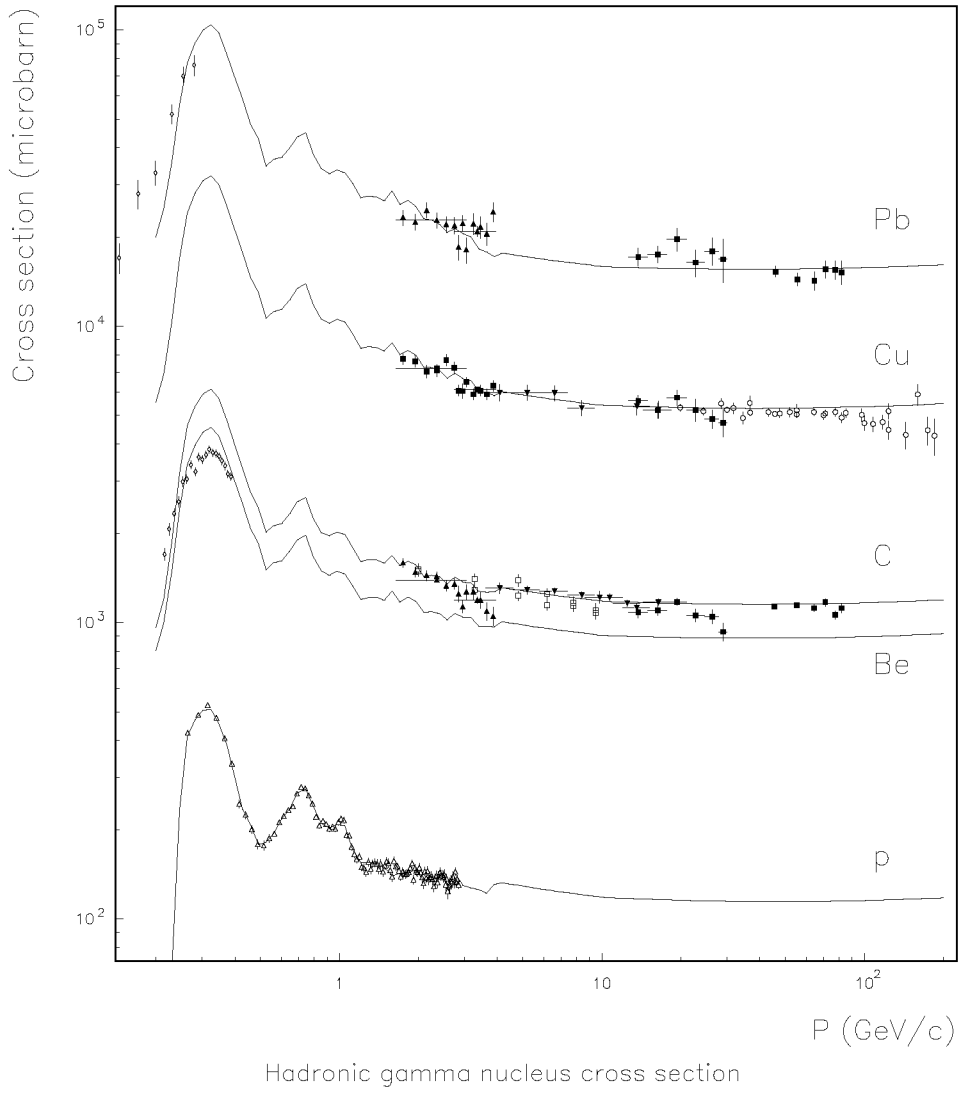

Figure 2.4: Gamma-nucleus hadroproduction cross sections.

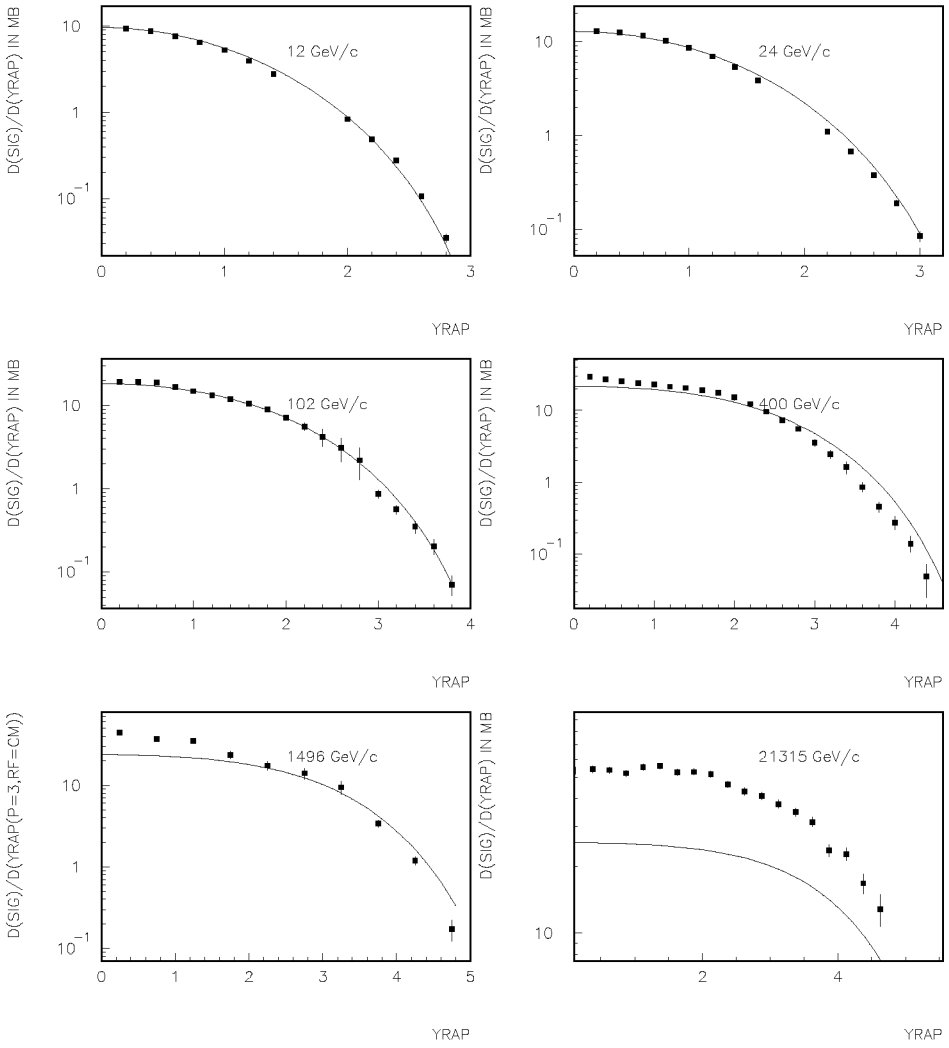

Figure 2.5: Rapidity distribution of negative pions in proton-proton collisions.

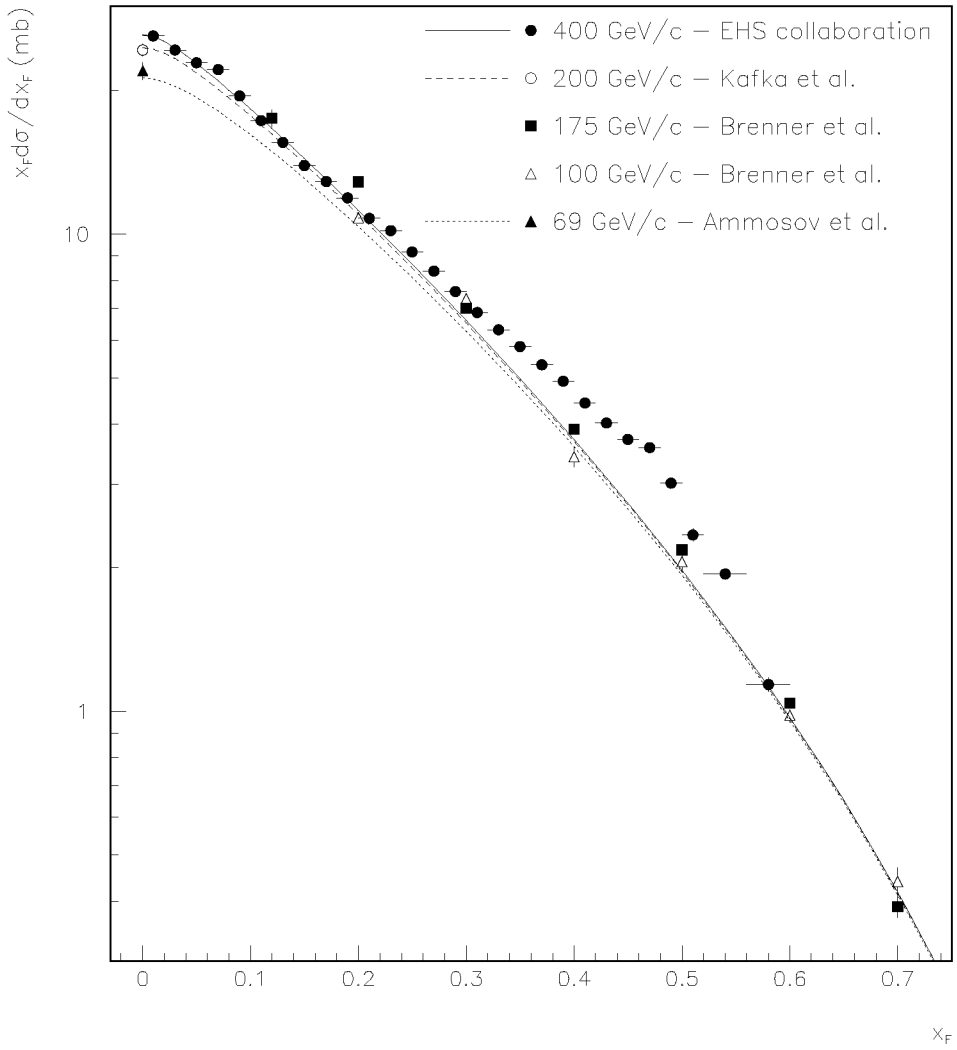

Figure 2.6: Momentum distribution of positive pions in proton-proton collisions.

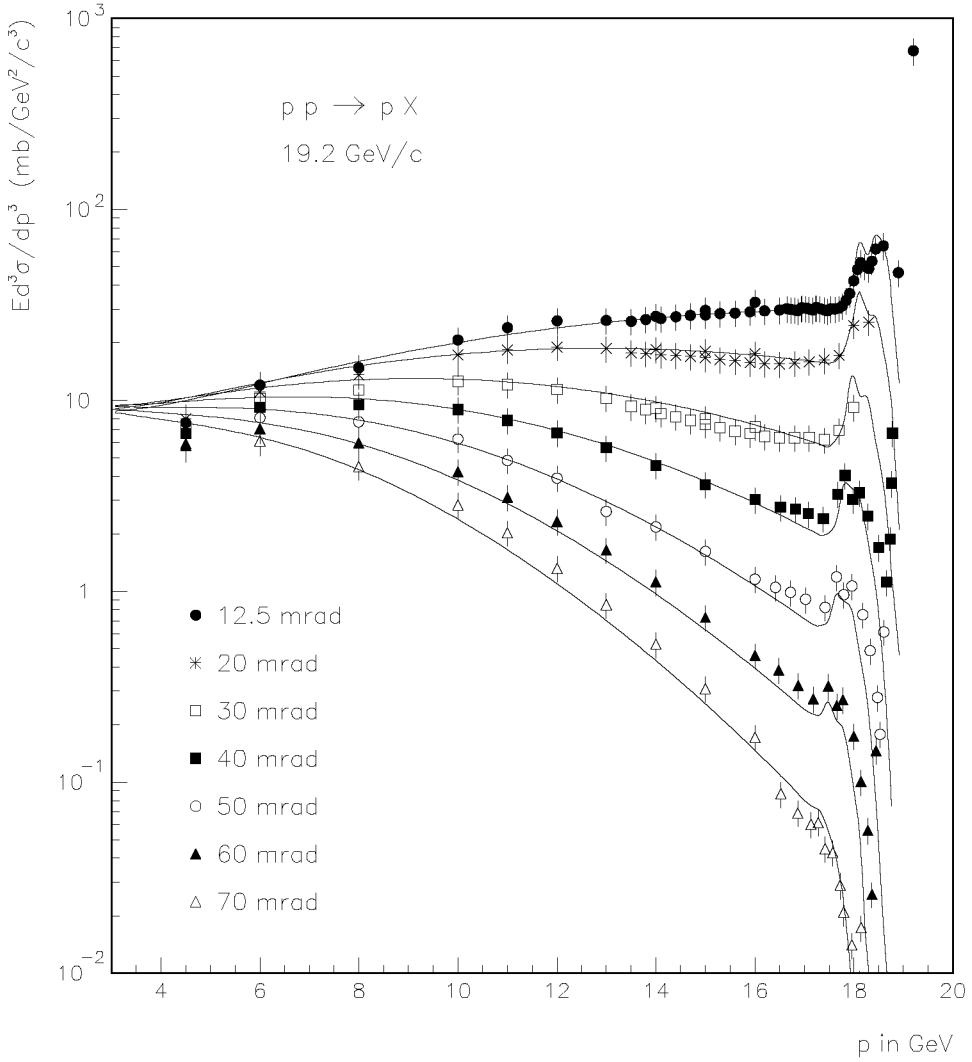

Figure 2.7: Proton spectra in proton-proton collisions.

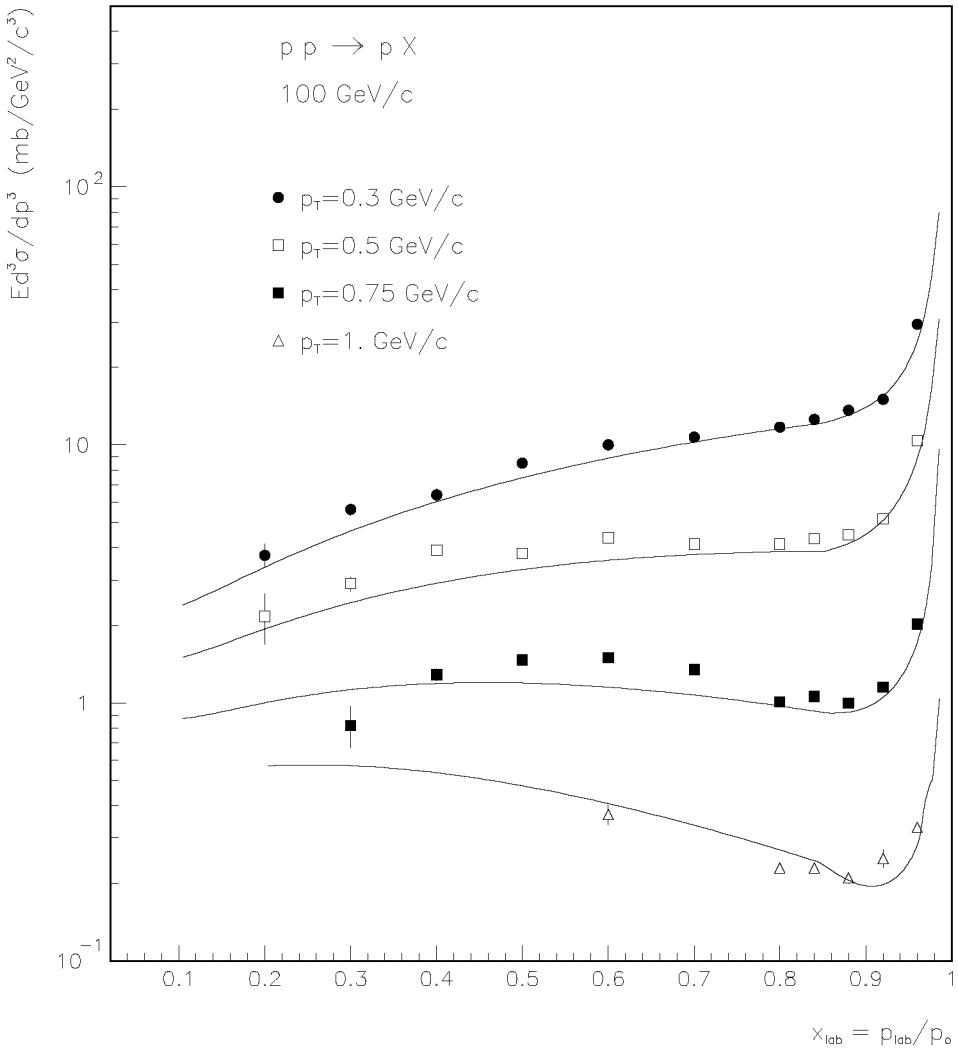

Figure 2.8: Proton spectra in proton-proton collisions.

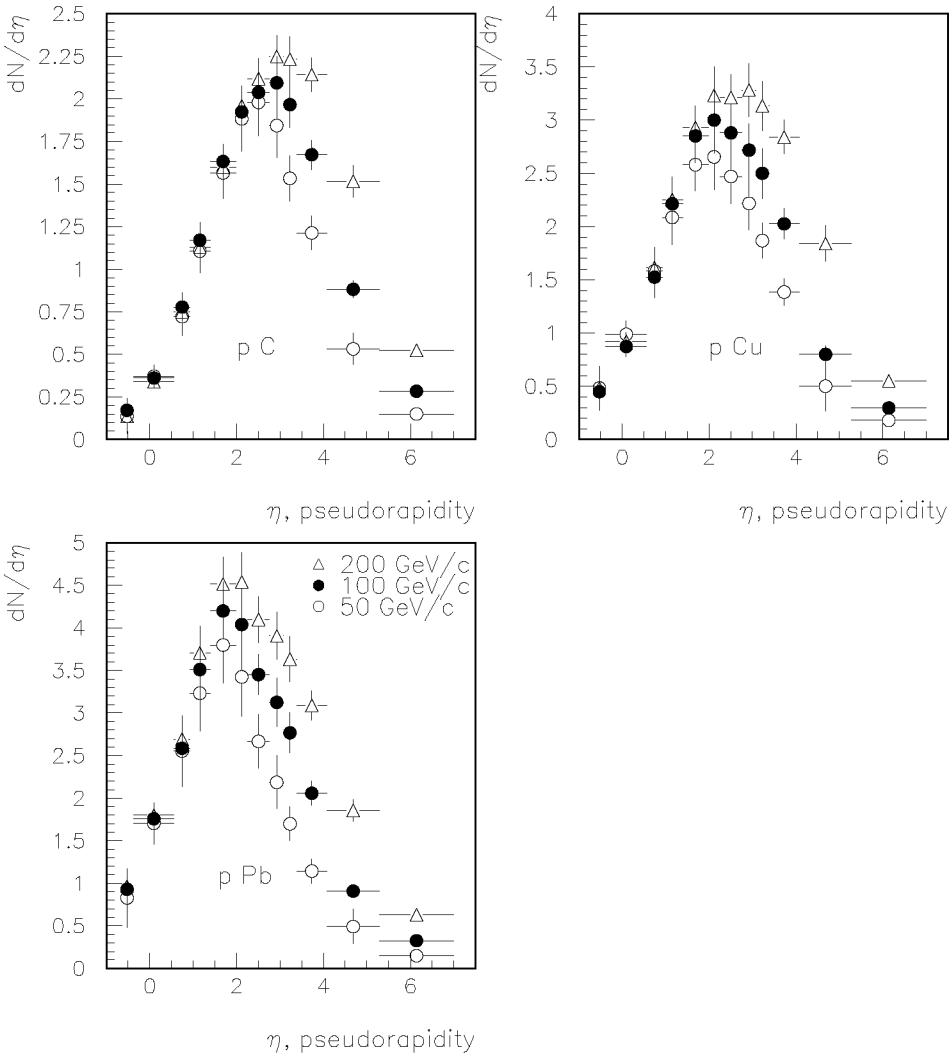

Figure 2.9: Shower particle production in proton-nucleus interactions *vs* pseudorapidity($\beta > 0.85$).

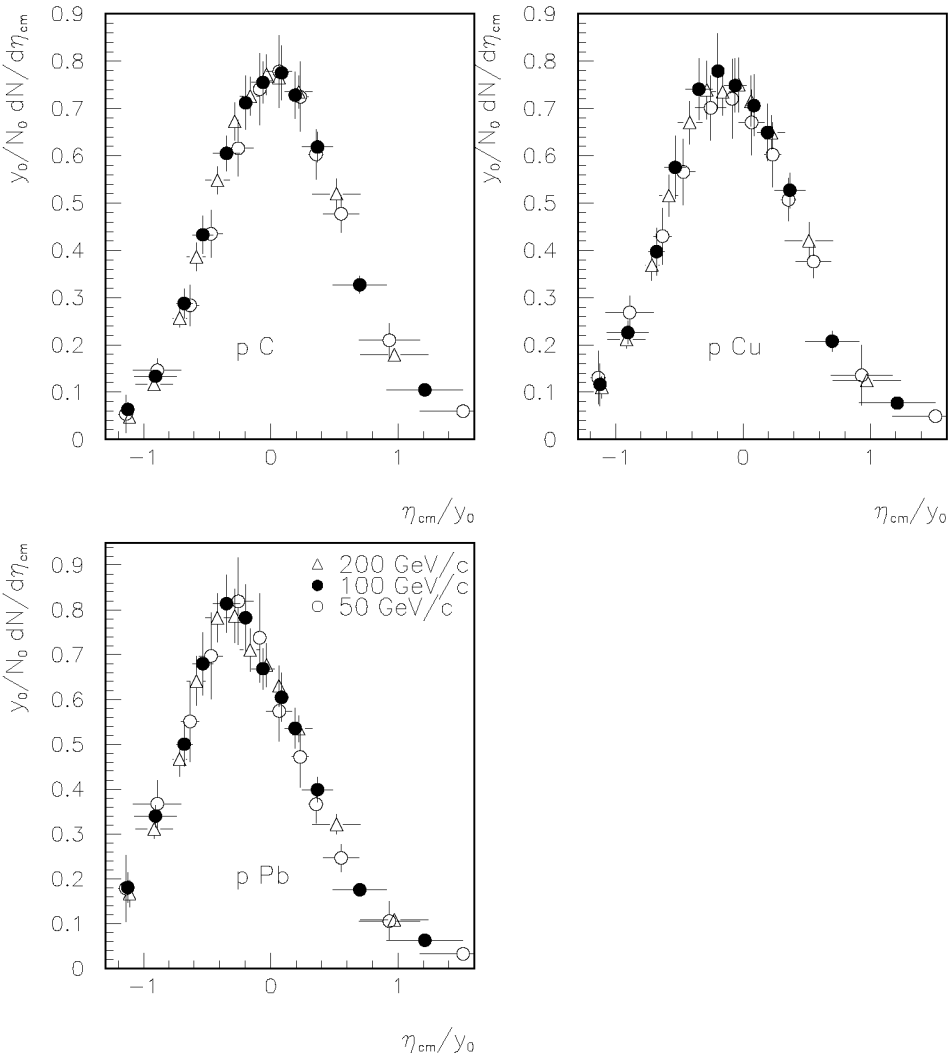

Figure 2.10: Shower particle production in proton-nucleus interactions in a scaling form ($\beta > 0.85$).

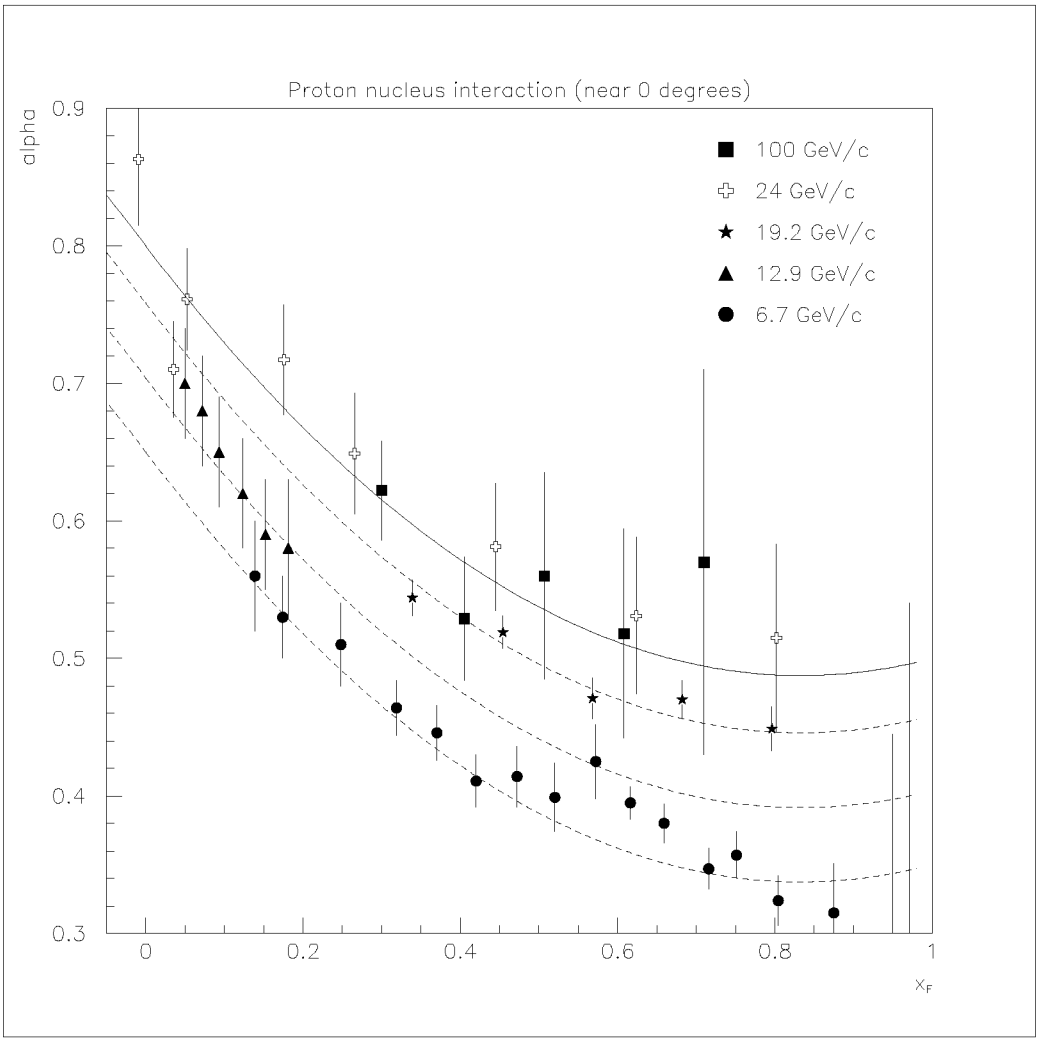

Figure 2.11: A-dependence of negative pion production in proton-nucleus interactions.

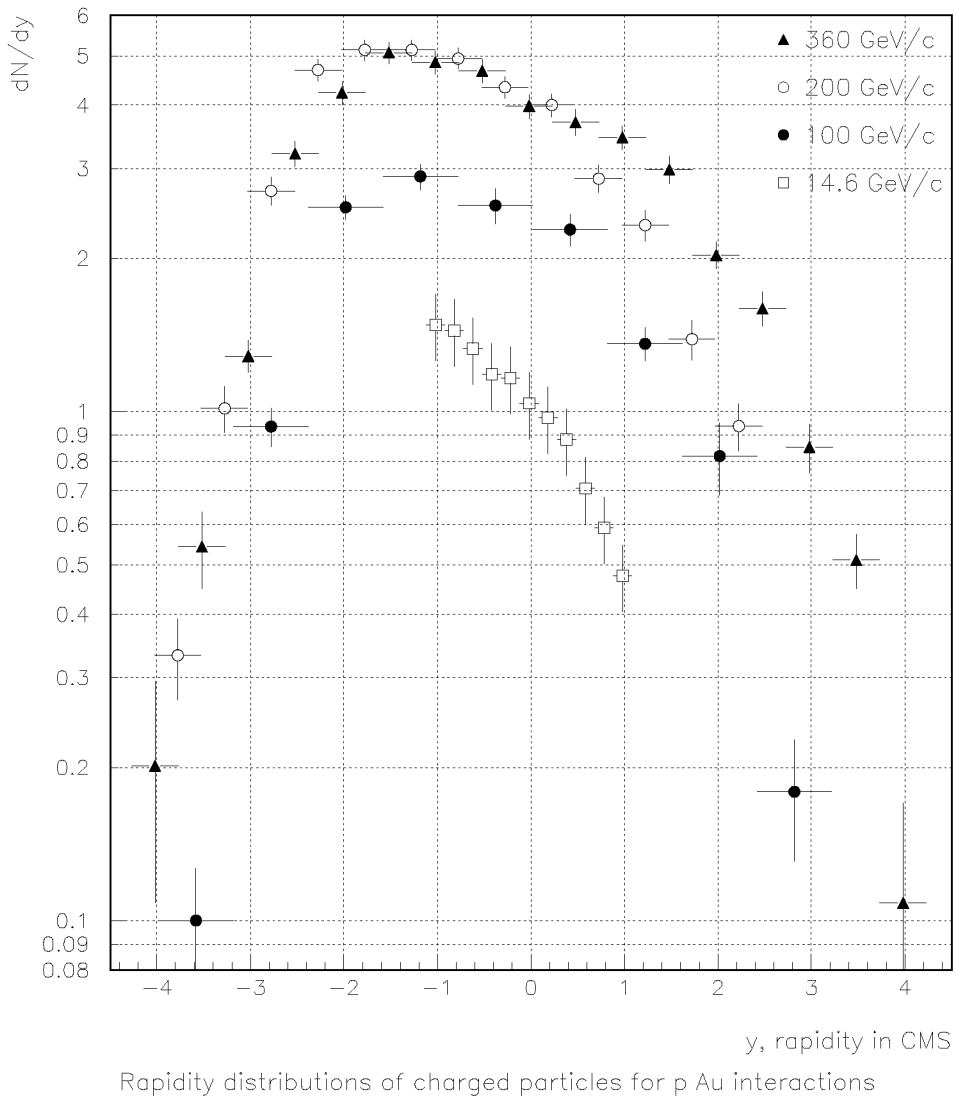

Figure 2.12: Rapidity distributions of charged particles in proton-nucleus interactions.

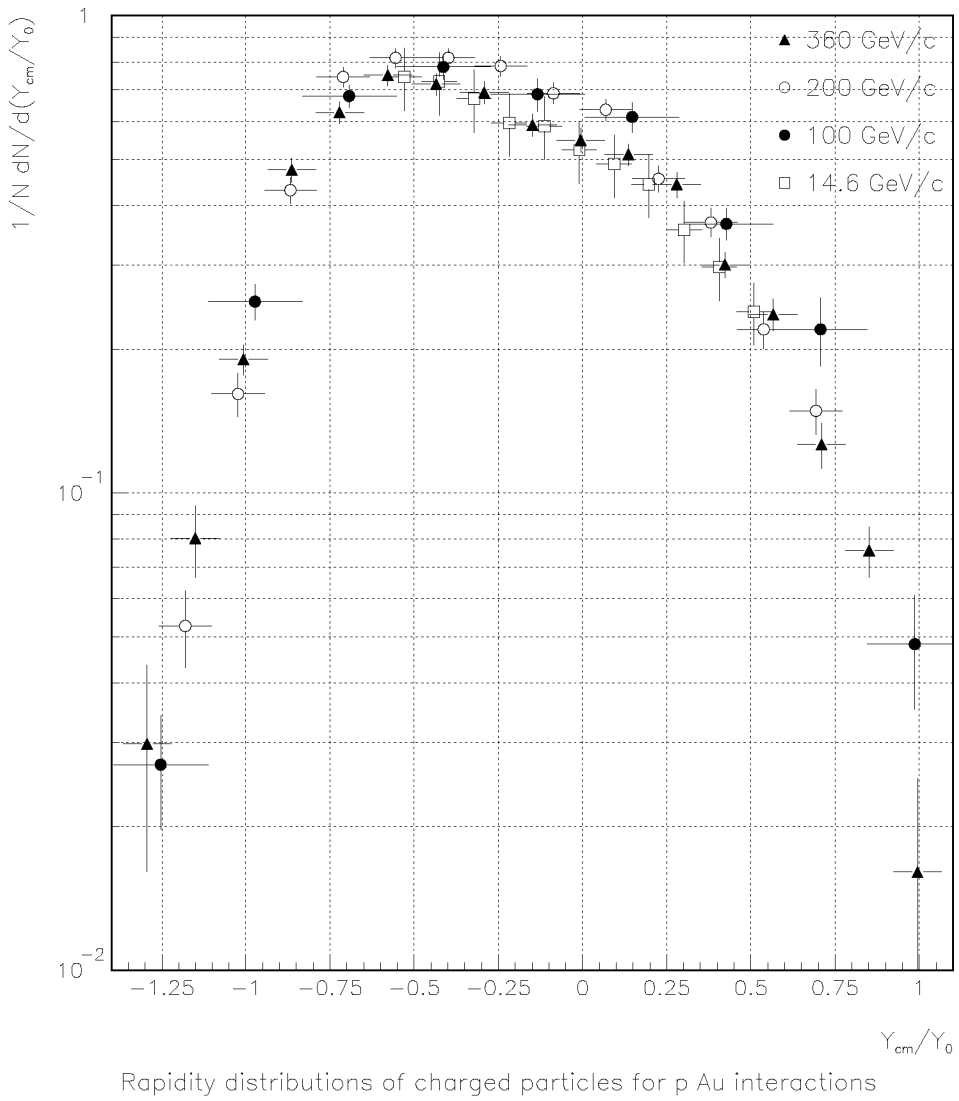

Figure 2.13: Scaling in rapidity distributions of charged particles in proton-nucleus interactions.

2.3 Benchmarking

Figs. 2.14 - 2.16 compare the MARS model with experimental data on average multiplicity of shower particles produced in proton-emulsion interactions. The model agrees well with data up to 800 GeV. Pseudo-rapidity distributions of fast charged particles in proton-nucleus collisions are shown in Fig. 2.17. The model agrees well with data for forward angles and somewhat underestimates the backward production.

Simulation of proton production is compared with data in Fig. 2.18. The model agrees well with data. Some adjustment of the A-dependence is probably needed at $x_F \sim 0.5$. Data on pion production and MARS calculations are compared in Fig. 2.19. The model agrees well with data, but decreases with $p_\perp$ faster than data.

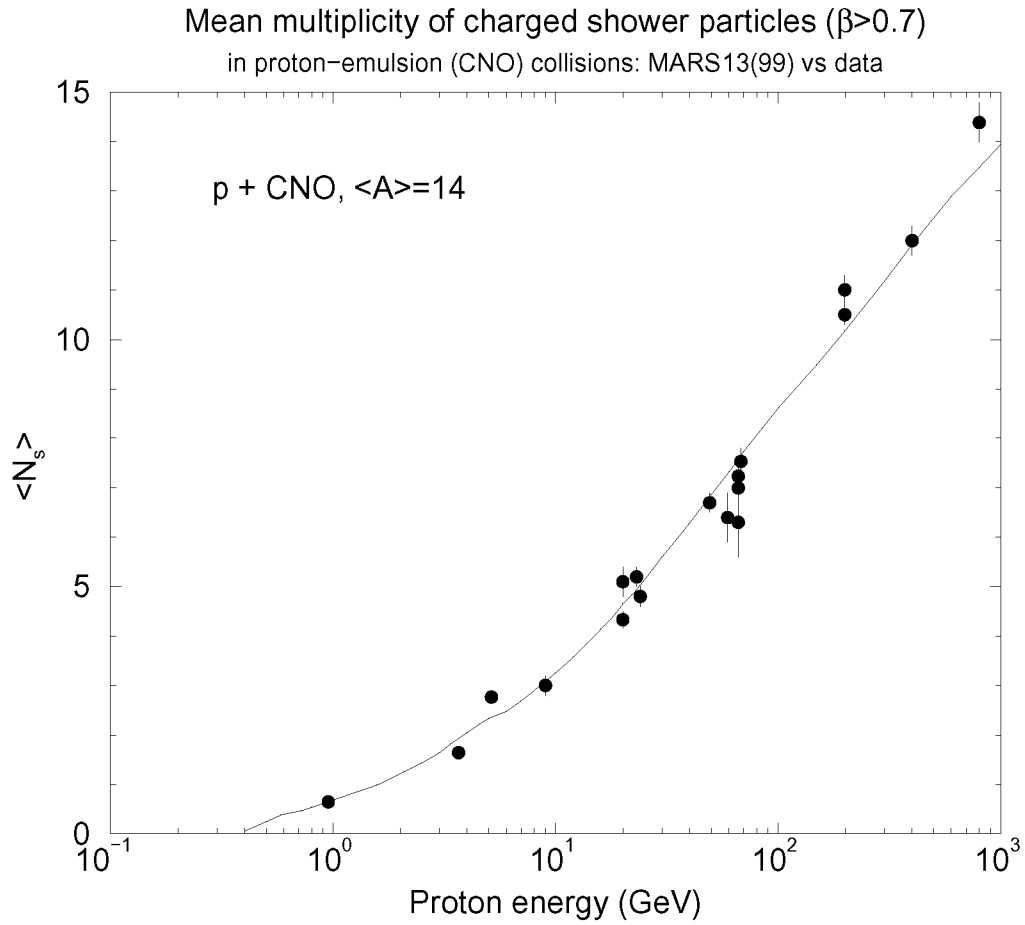

Figure 2.14: Mean multiplicity of shower particles in interactions of protons with light nuclei in emulsion.

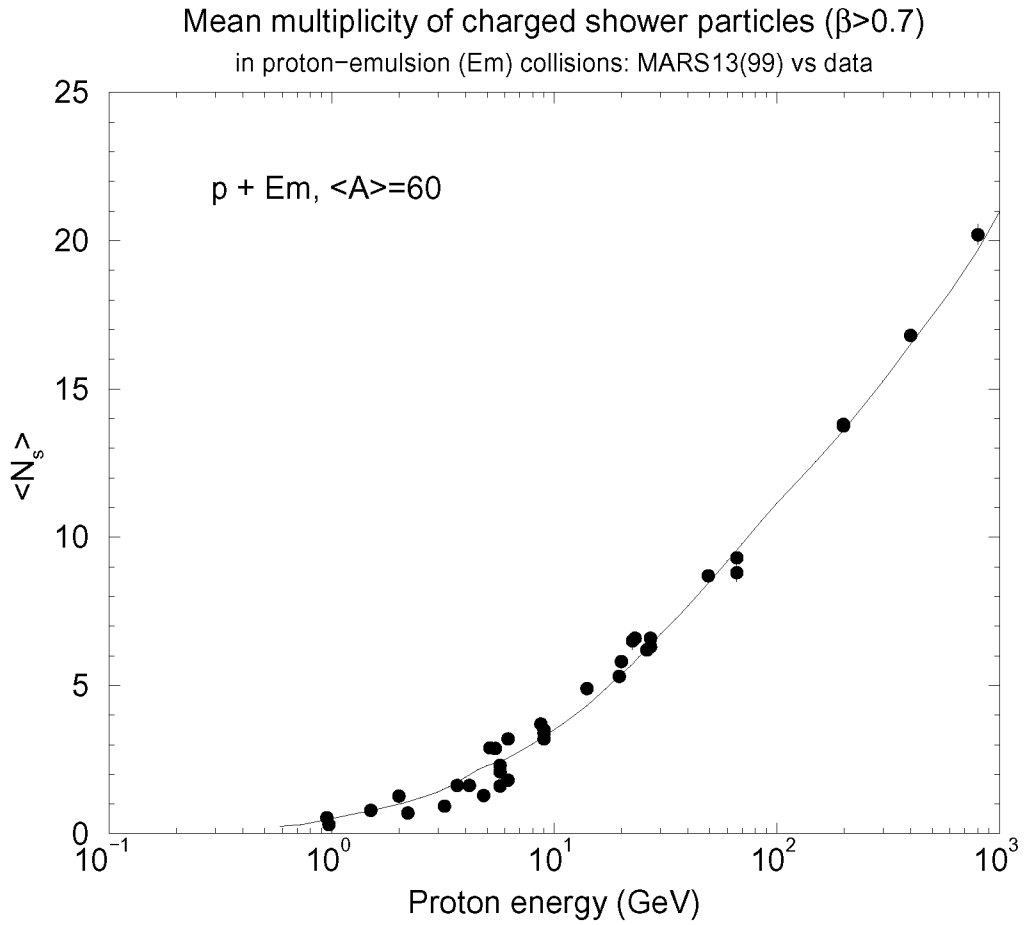

Figure 2.15: Mean multiplicity of shower particles in interactions of protons with medium nuclei in emulsion.

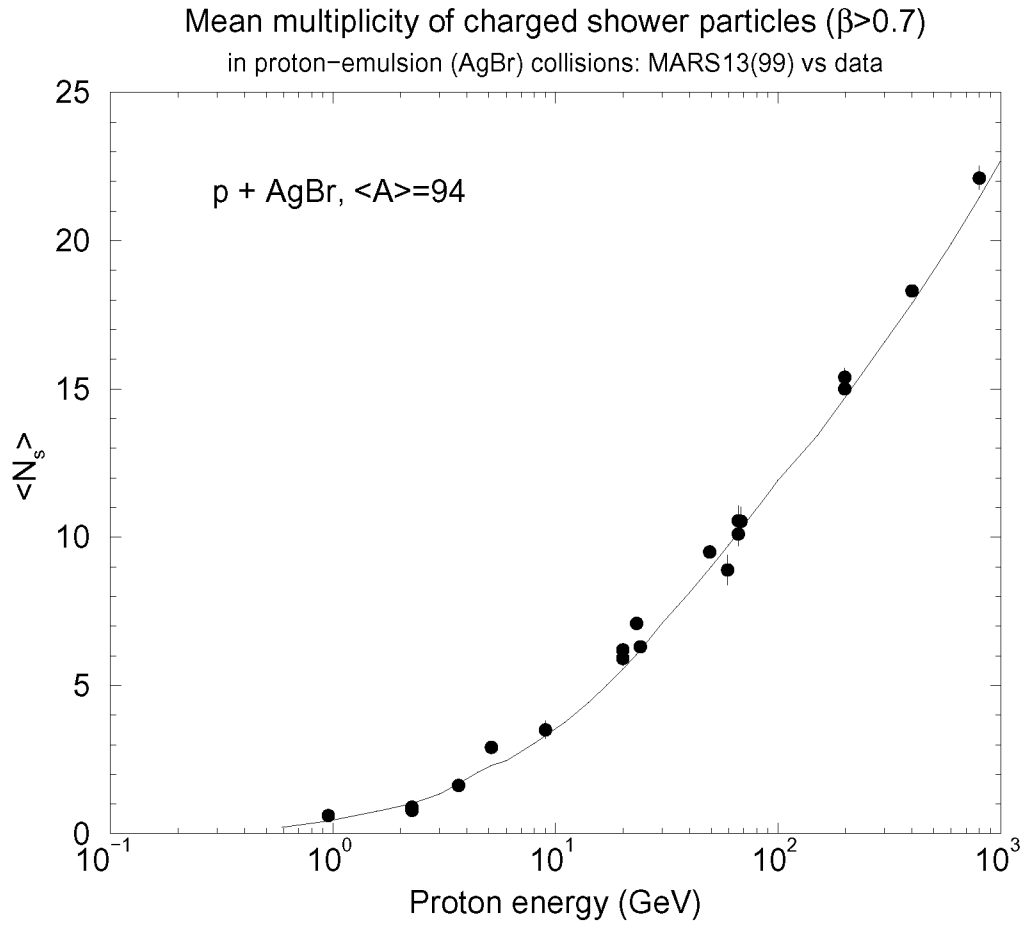

Figure 2.16: Mean multiplicity of shower particles in interactions of protons with heavy nuclei in emulsion.

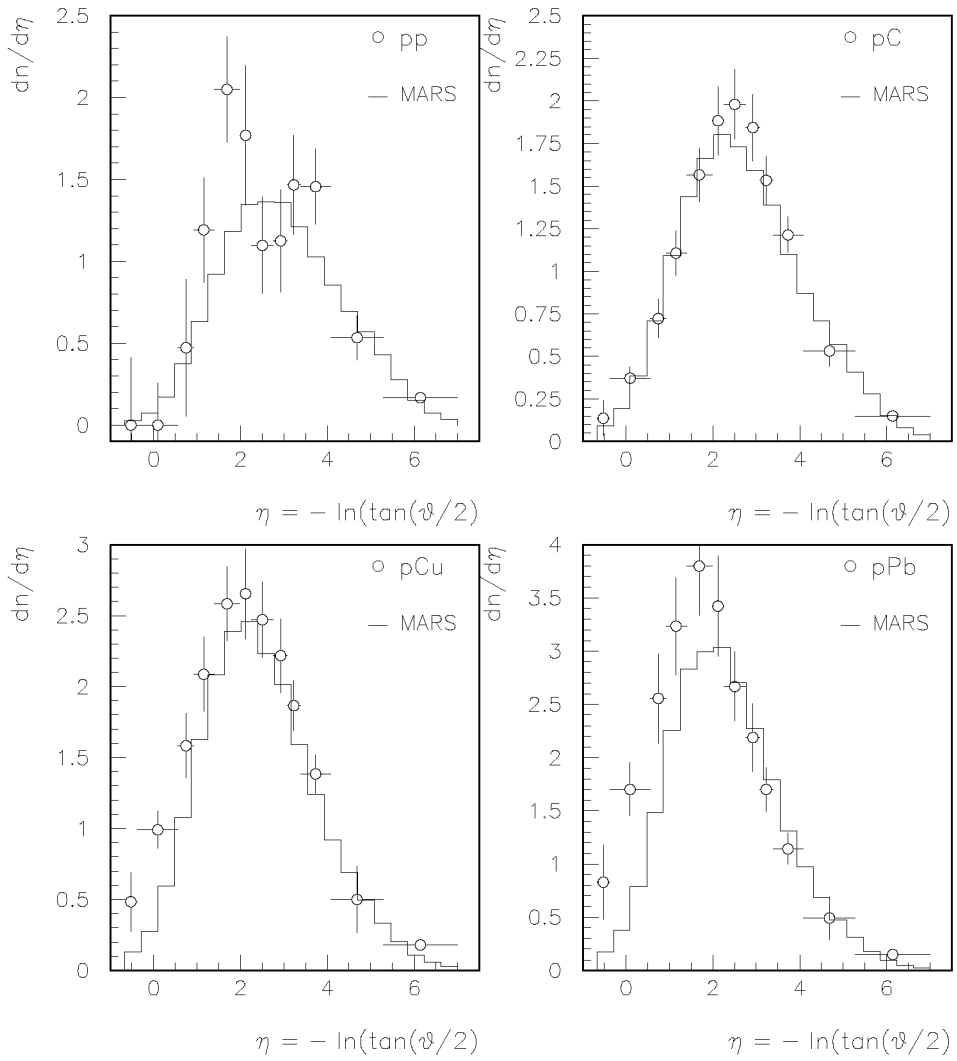

Figure 2.17: Charged particle production in proton-nucleus interactions at 50 GeV ($\beta > 0.85$).

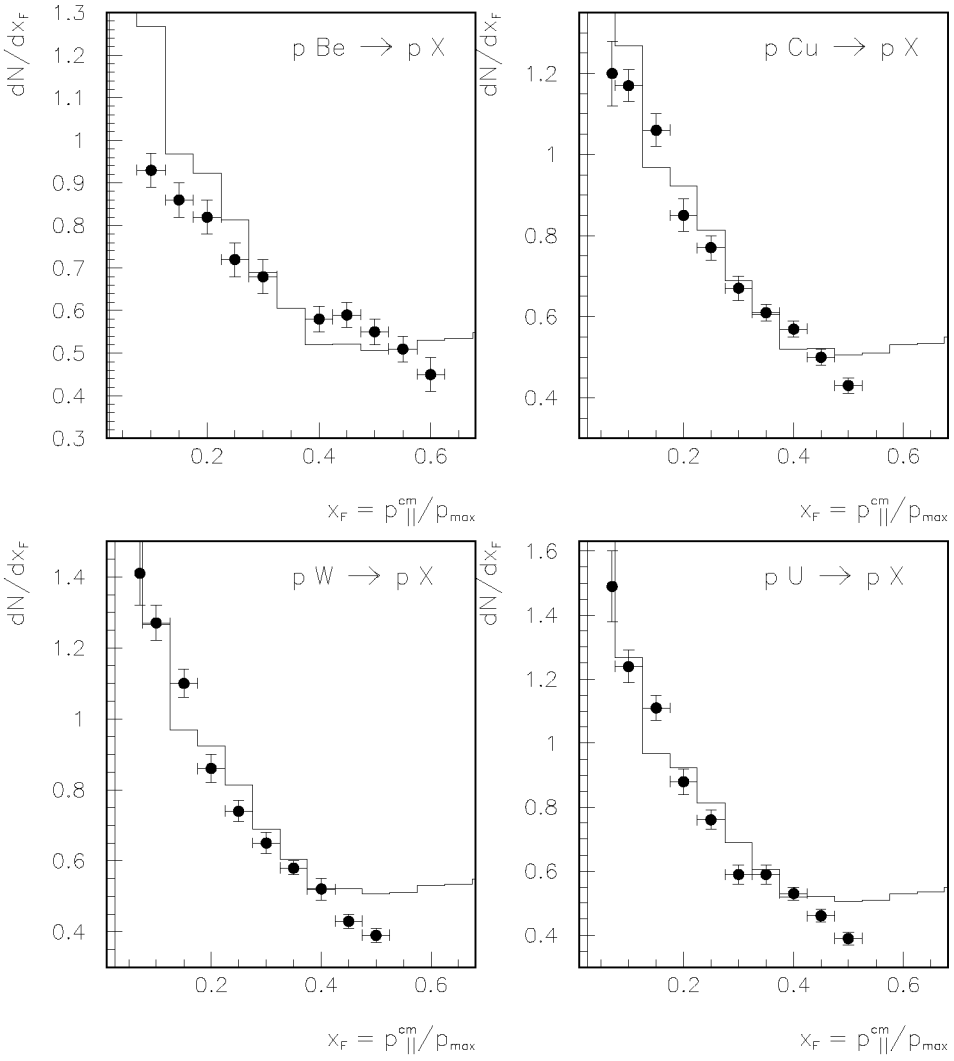

Figure 2.18: Proton production in proton-nucleus interactions at 120 GeV/c.

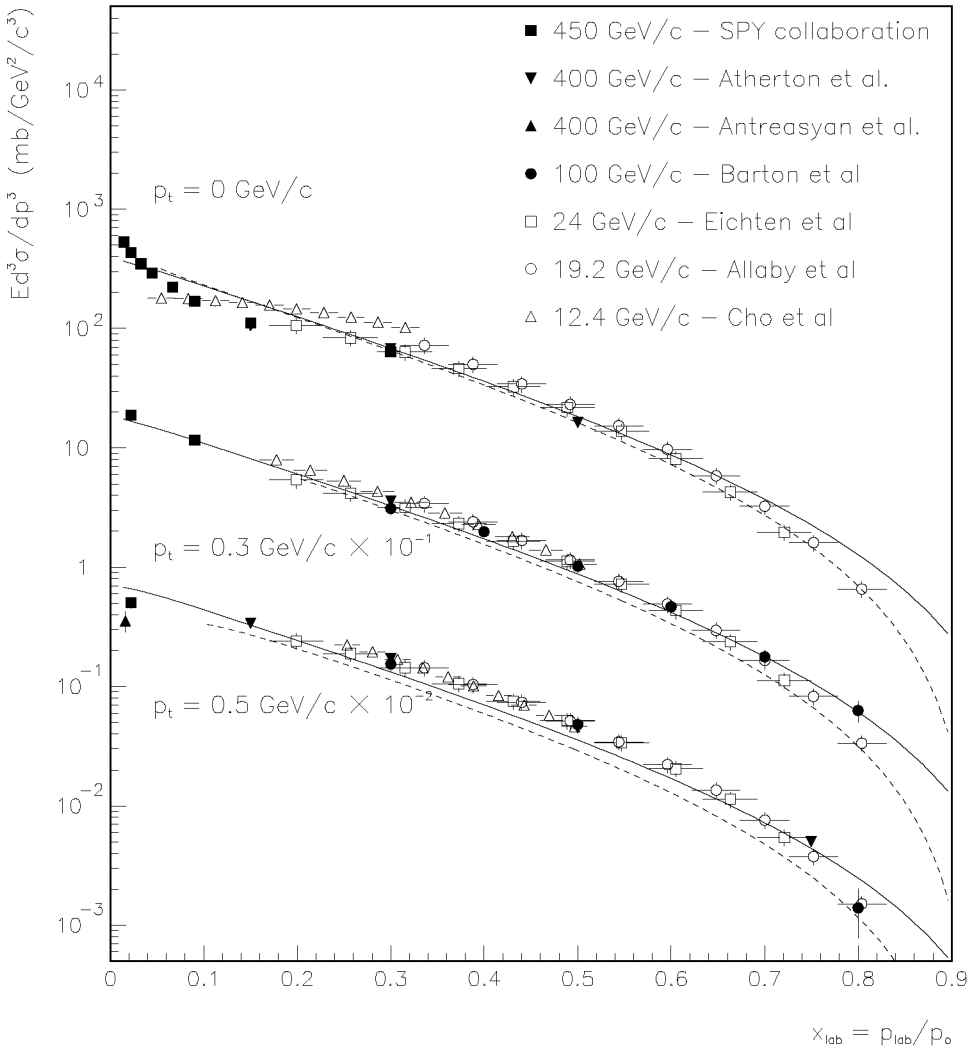

Figure 2.19: π^+ production in proton-beryllium interactions.

2.4 Implementation into LAHET

To generate hadron-nucleus inelastic interactions using the MARS hadron production module in the LAHET framework, one needs to call subroutine

MARS_hA_inelastic(ityp,ecl,a1,z1,nopart,kind,alpha,beta,gam,ep,wtfas,exout1,exout2,exwout2).

INPUT PARAMETERS:
ityp - initial particle type (LAHET convention),
ecl - kinetic energy of this particle in MeV,
a1 and z1 - atomic mass and number of target nucleus.

OUTPUT PARAMETERS:
nopart - a number of generated secondary particles,
kind - an array of generated particle types,
alpha,beta,gam - arrays of created particle angles (LAHET convention),
ep - an array of kinetic energies of secondaries in MeV,
wtfas - an array of weights of secondaries,
exout1 - evaporated heavy fragment and recoil energy of nucleus in MeV,
exout2 - an energy of an inclusive photon after de-excitaion in MeV,
exwout2 - a weight of such a photon.

In the LAHET routine cascad.f, one has to add **call fmars(ecl,a1,z1)**. An inelastic collision will be generated and information about secondaries will be returned to **common/banka/**.

MARS_ha_inelastic calls:

- MARS_ha_init to prepare some constants,
- SIGLAM to calculate inelastic and production cross sections,
- TREEM to generate secondaries.

All needed routines are collected in files m14eve5.f, m14evepi.f, m14cem.f, m14util-short.f, fmars.f.

2.5 Verification

We have simulated proton-carbon and proton-tantalum interactions at 10 GeV/c using the MARS model implemented into LAHET, the standard MARS generator and the FLUKA model implemented into LAHET. The calculated results and experimental data on proton and pion production are presented in Figs. 2.20 - 2.21. Results obtained with the MARS model do not depend on framework.

Energy deposition of 50 GeV proton in a tungsten rod was simulated by means of LAHET using the FLUKA and MARS generators. This calculations are compared in Fig. 2.22 with results obtained using the original FLUKA and MARS codes and last year simulation with LAHET(FLUKA) with handling gammas with MCNP. LAHET(MARS) and LAHET(FLUKA) agree within 10%. It is not decided yet how to work with excitation energy and photon produced by the MARS generator in the LAHET framework. Absence of this component in the current setup results in some underestimation of energy deposition in the LAHET(MARS) simulation.

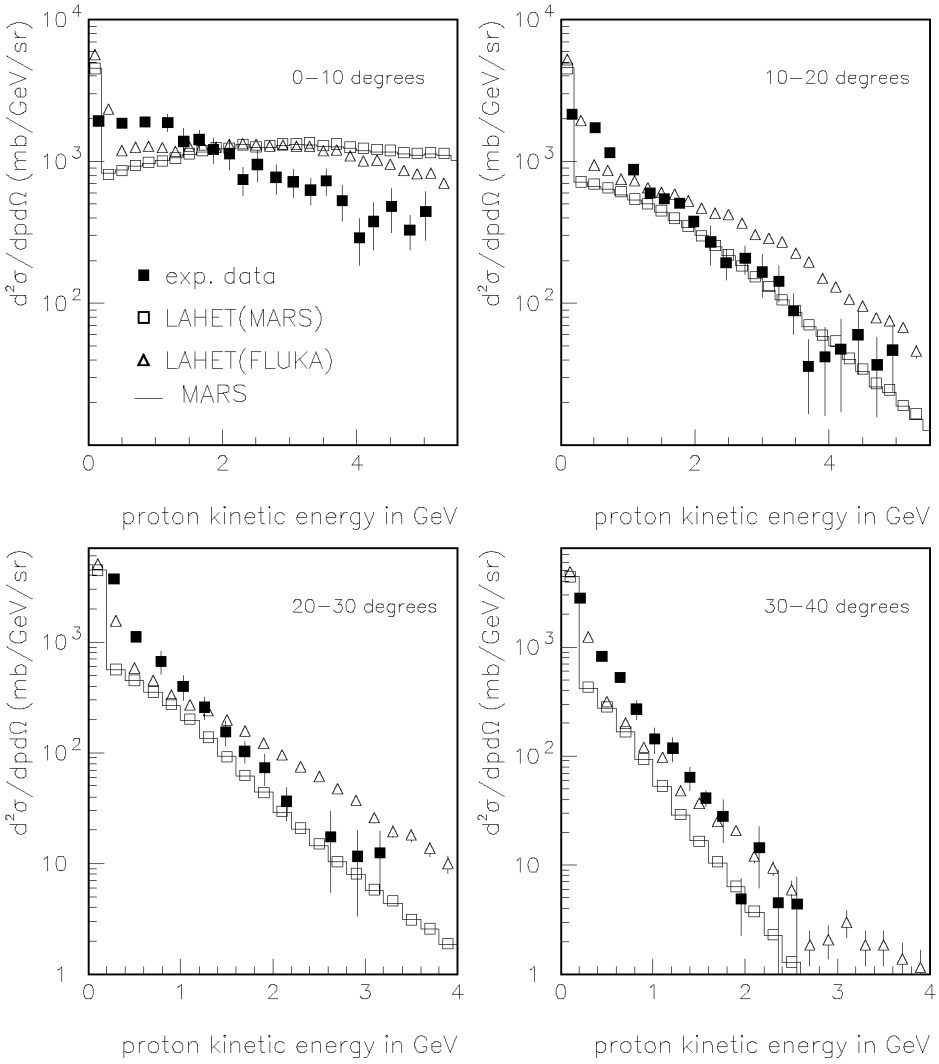

Figure 2.20: Proton-tantalum interactions at 10 GeV/c.

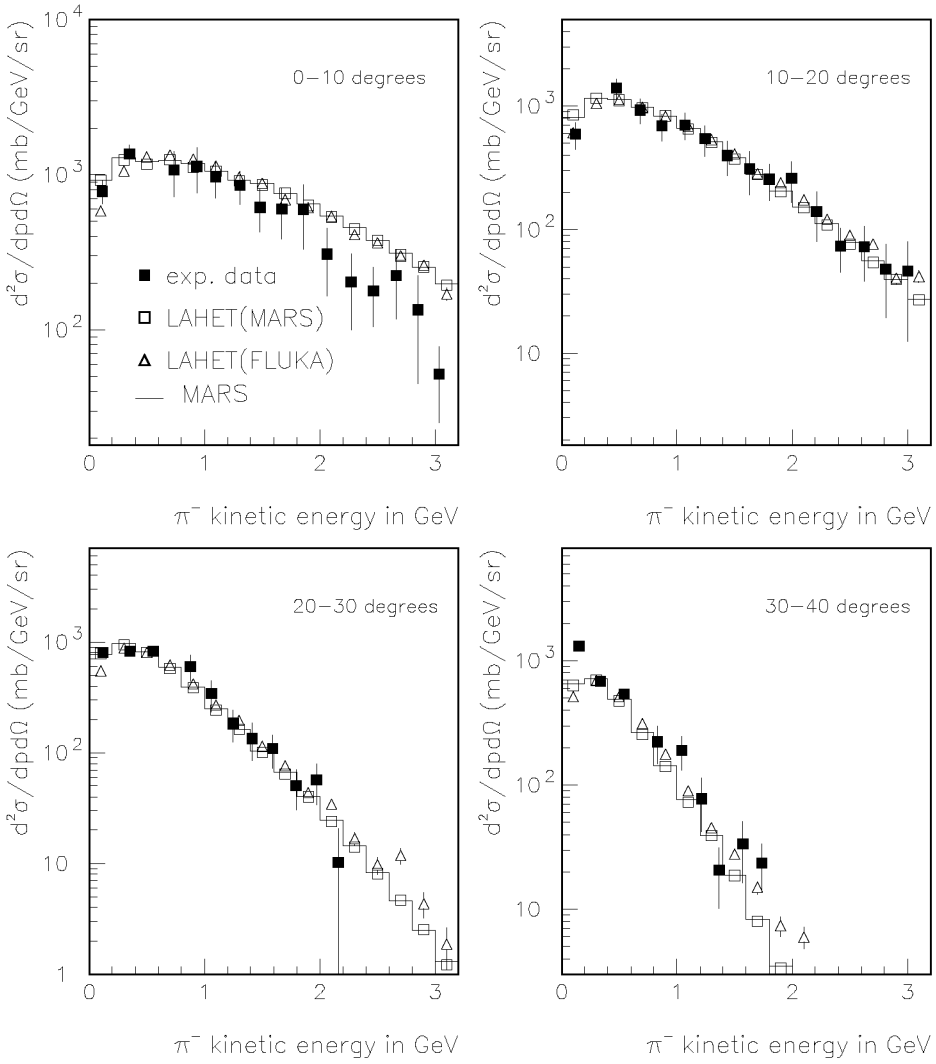

Figure 2.21: Proton-tantalum interactions at 10 GeV/c.

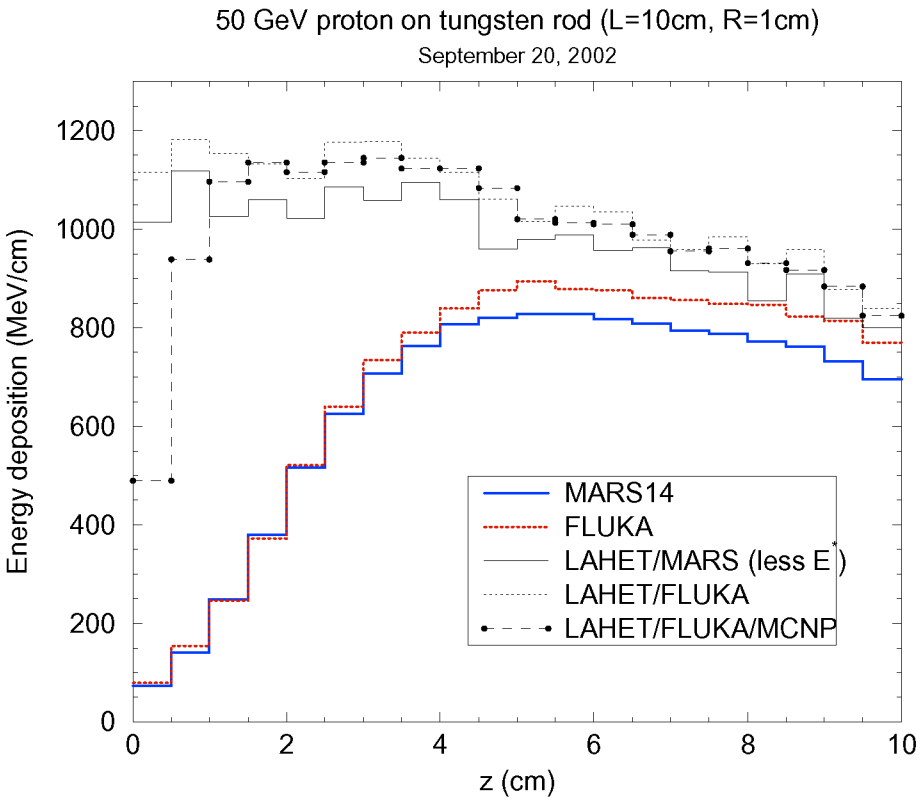

Figure 2.22: Energy deposition in tungsten rod irradiated by 50 GeV protons.

Chapter 3

Multiple Coulomb Scattering Model

3.1 Analytical methods to calculate multiple Coulomb scattering

The angular distribution after a charged particle passage through a scatterer of length t, can be written as

$$F(\theta, t) = \frac{1}{2\pi} \int_0^\infty J_0(p\theta) exp(-tA(p)) p dp, \tag{3.1}$$

where

$$tA(p) = t \int_0^\infty d\Omega (1 - J_0(p\theta)) \frac{d\Sigma}{d\Omega}, \tag{3.2}$$

here $\frac{d\Sigma}{d\Omega}$ is a single scattering differential cross-section.

If thickness t is large enough, then

$$tA(p) = \frac{p^2}{4} < \theta^2 > - \frac{p^4}{64} < \theta^4 >, \tag{3.3}$$

where

$$< \theta^k >= t \int_0^\infty d\Omega \theta^k \frac{d\Sigma}{d\Omega}$$

In this case the angular distribution could be rewritten in a simple form

$$F(\theta, t) = \frac{1}{\pi < \theta^2 >} e^{-z} (1 + D(1 - 2z + \frac{z^2}{2})), \tag{3.4}$$

where $z = \frac{\theta^2}{<\theta^2>}$ and $D = \frac{<\theta^4>}{2<\theta^2>^2} \sim 1/t$. For a scatterer length t large enough, $D \sim 0$ and a near-Gaussian distribution (3.4) coincides with the Rossi formula [4].

If one uses a Moliere differential cross section [5] with a Gaussian nuclear form-factor, the exact solution of equation (3.1) can be obtained [6]. For such a cross section, it is possible to compare known approximations of angular distributions the with precise results. In Fig. 3.1, five approaches are presented and compared with the exact calculations for different lengths of the scatterer:

- Moliere distribution [5];
- modified Moliere distribution which takes into a account nuclear form-factor for a small scatterer thickness [6];
- Gaussian distribution, (3.4) with $D = 0$;
- Near-Gaussian distribution (3.4) (Gaussian+1) ;
- Distribution (3.4) with an additional term in series (Gaussian+2);

It is seen that the modified Moliere distribution [6] could be used for calculation with a ~10% accuracy for $D > 0.05$. A near-Gaussian distribution (3.4) agrees with the exact calculation for $D \leq 0.01$ within a few percent. Adding an additional term in series (3.4) slightly improves accuracy.

3.2 Unified Monte Carlo algorithm

Two methods are widely used for simulation of multiple Coulomb scattering (MCS): sampling from Moliere [5] and Gaussian [4] distributions. Limits of applicability of these approaches were determined in [6], where the Moliere theory of MCS was modified to take into account a nuclear screening. It was shown that the angular distribution obtained in such a way coincided with the Moliere one for the thicknesses of 0.1 - 1 radiation lengths and reached the Gaussian asymptotic for 100 - 1000 radiation lengths. Note, that the convolution step-by-step of the Moliere distribution never becomes a Gaussian. It was shown [7] that in some cases the use of Moliere and Gaussian distributions can lead to quite large errors in Monte-Carlo simulations. The sampling algorithm [6] which takes into account the nuclear screening was proposed, but unfortunately it was based on the assumption of a Gaussian approximation for the nuclear form-factor, which is not accurate for heavy nuclei.

A non-trivial approach for sampling from Moliere distribution was proposed in [8, 9]. The region for a single scattering differential scattering cross-section was divided into two parts: $\theta < \theta_{max}$ and $\theta > \theta_{max}$. The small angle scattering was sampled using a quasi-Rossi Gaussian approximation, while rare events with large angle scattering were

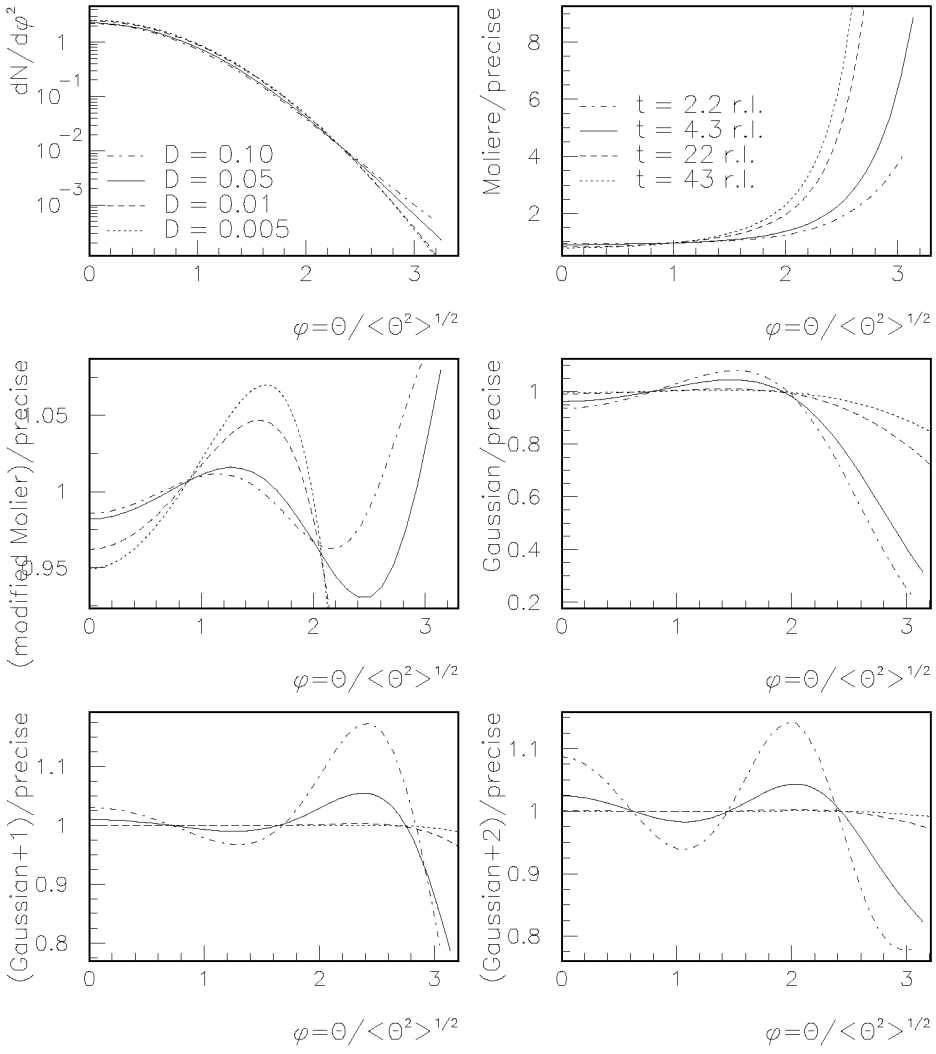

Figure 3.1: Angular distributions after uranium absorber.

generated using a discrete interaction cross-section. The threshold parameter θ_{max} was chosen using a non-exact semi-numerical evaluation. Here we propose another method for threshold parameter estimation which gives an ability to simulate MCS distribution with about a percent accuracy for any step size and takes into account nuclear screening with an arbitrary form-factor.

Let's split formula (3.2) into small-angle and large-angle parts

$$tA(p) = t\int_0^{\theta_{max}} d\Omega(1 - J_0(p\theta))\frac{d\Sigma}{d\Omega}$$

$$+\int_{\theta_{max}}^{\infty} d\Omega(1 - J_0(p\theta))\frac{d\Sigma}{d\Omega} \tag{3.5}$$

To avoid dependence on a particular form-factor, let's choose upper limit as

$$\theta_{max}^2 < 0.1 \cdot \theta_{nuc}^2, \tag{3.6}$$

where θ_{nuc}^2 is equal to $3/(P_0^2 \cdot r_{nuc}^2)$, P_0 is an incident particle momentum and r_{nuc}^2 is an average nucleus radius squared. In this case, the first term in (3.5) can be rewritten as

$$\Phi_1(p) = \chi_c^2 p^2(B - p^2\theta_{max}^2/16 + \cdots)/4, \tag{3.7}$$

where parameter names and values are taken from the Moliere theory

$$\chi_c^2 = 0.6008Z^2 m_e^2 \rho t/(P_0^2\beta^2 A),$$

$$\chi_a = 1.063\sqrt{1. + (Z/75\beta)^2}/(r_a P_0),$$

where Z and A are target charge and mass, respectively, m_e is an electron mass, β is a velocity, ρ is a target density, $r_a = 0.885/(Z^{1/3}\alpha m_e)$ and $B_G = \log(\theta_{max}^2/\chi_a^2) - 1$. If one takes into account terms proportional to p^4 only in the series (3.5), it gives the following approximation for the "soft" distribution F_1

$$F_1(\theta, t) = \frac{1}{\pi\theta_1^2} exp(-z^2)(1 + D(1 - 2z^2 + z^4/2)), \tag{3.8}$$

where $\theta_1^2 = B_G\chi_c^2$, $z^2 = \frac{\theta^2}{\theta_1^2}$ and $D = \frac{\theta_{max}^2}{2B\theta_1^2}$.

If D is small enough, the "soft" distribution reaches a near-Gaussian asymptotic. For an arbitrary step size, one can calculate θ_0 from the equation

$$D = \frac{2y}{(\log y + R)^2} = \delta \ll 1 \tag{3.9}$$

where

$$R = \log(\chi_c^2/\chi_a^2) - 1$$

and

$$y = \theta_0^2/\chi_a^2.$$

It's quite easy to find a threshold value for θ_0 from the non-linear equation

$$y = 2\delta(\log y + R)^2. \tag{3.10}$$

Using a simple anzatz, $y \to 8\delta x^2$, where $\delta \ll 1$ is a parameter, one can get a Moliere-like non-linear equation

$$x - \log x = \frac{1}{2}\log\frac{8\delta\chi_c^2}{\chi_a^2 e} \tag{3.11}$$

One can use any approximate solution for the above equation. The simple one is the following formula which gives a solution approximation with a 10% accuracy

$$x = \frac{b}{2}(1 + \frac{\log b}{b-1})(1 + \sqrt{1 - \frac{1}{b}}), \tag{3.12}$$

where

$$b = \frac{1}{2}\log\frac{8\delta\chi_c^2}{\chi_a^2 e}.$$

The derivation between the exact solution and approximate one can be considered as a redefinition of δ.

If one chooses $\theta_{max}^2 = min(\theta_0^2, \theta_{nuc}^2/10)$, the first small-angle distribution can be sampled using (3.8) , while the second distribution can be simulated as a number of discrete interactions. The average number of discrete interactions is simply

$$N_{disc} = \Sigma(\theta > \theta_{max})t \sim \chi_c^2/\theta_{max}^2. \tag{3.13}$$

For a large step size $\theta_{max}^2 = \theta_{nuc}^2/10$. Thus, in the worst case, one has $N_{disc} = 10\chi_c^2/\theta_{nuc}^2$. It was already shown that in the case of $D = \theta_{nuc}^2/(2B_G^2\chi_c^2) < 0.01$, the angular distribution can be described by a near-Gaussian approximation (3.4). Therefore, the average number of discrete interactions has the upper limit equal to $\Sigma(\theta > \theta_{max})t \leq 500/B_G^2$. Usually, B_G is about 20 or so, thus the actual number of discrete interactions is not large.

For a small step size, $\theta_{max} = \theta_0$. Equation (3.11) has a solution if

$$b = \frac{1}{2}\log(\frac{8\delta\chi_c^2}{\chi_a^2 e}) \geq 1. \tag{3.14}$$

For a smaller step size, the maximal possible value of the parameter δ is chosen as

$$\delta = \frac{e^3\chi_a^2}{8\chi_c^2}.$$

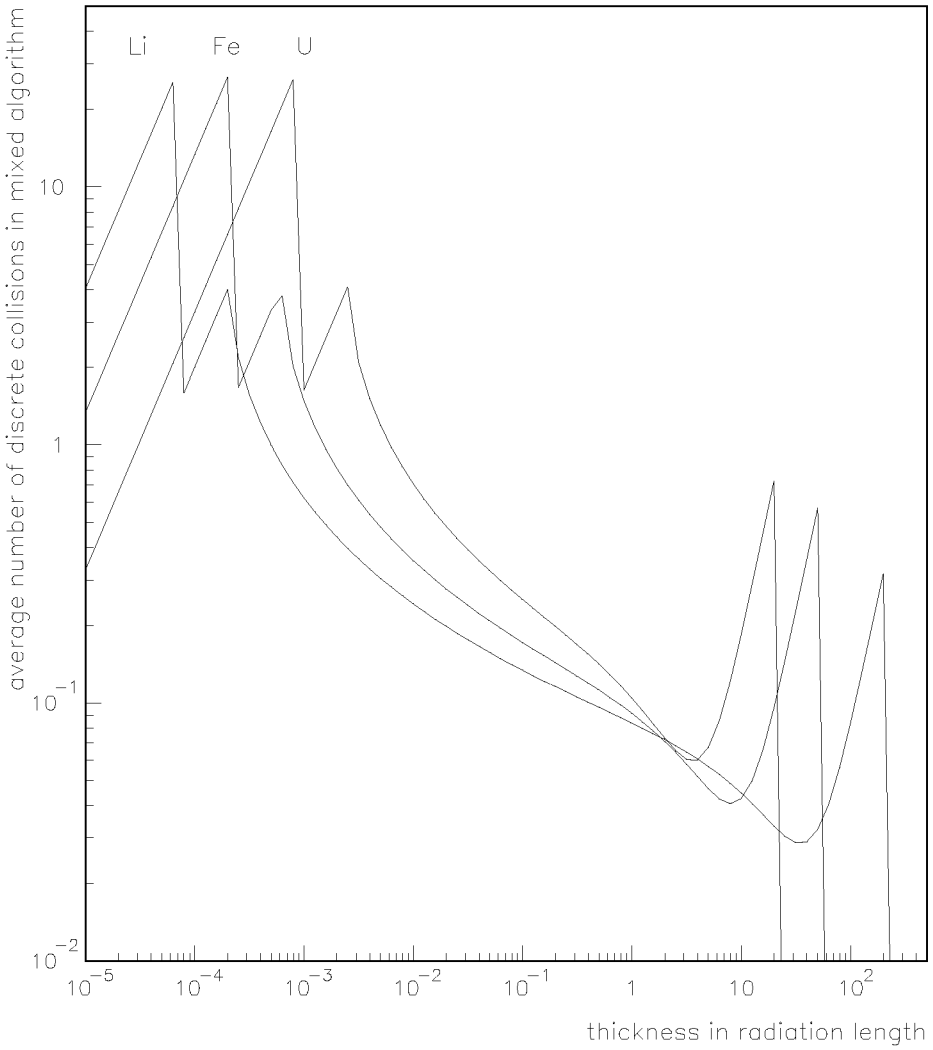

Figure 3.2: A number of discrete interactions in the unified algorithm, $\delta = 0.03$

For such a small distance, the number of discrete collisions to be sampled reaches a value of about 10. The real number of discrete collisions are shown on in Fig. 3.2. One can see that the actual number of discrete collisions $N_{dis} \sim 1$.

In summary, to simulate an angular deflection on a step t one should proceed with the following:

- If the step size t is large enough and condition $\theta^2_{nuc}/(2B^2_G\chi^2_c) < 0.01$ is satisfied, one samples an angle from the near-Gaussian distribution (3.4).

- If the step size t is smaller, then one calculates θ_0. If condition (3.14) is satisfied, one obtains θ_0 solving the nonlinear equation (3.11), otherwise one redefines δ as $\frac{e^3\chi^2_a}{8\chi^2_c}$ and puts x to be equal to 1.

- From (3.8) the "continuous" small-angle scattering is sampled.

- The actual number of discrete interactions is simulated from a Poisson distribution with the mean of N_{disc}.

- Discrete interactions are sampled using the "true" single scattering differential cross-section. An arbitrary nuclear form-factor can be included by acceptance-rejection method with a high efficiency because the minimal angle is rather small (see (3.6)).

- "Continuous" and discrete interaction angles are properly added in order to produce the total scattering angle on the step t.

It is seen from Fig. 3.3, that for $\delta = 0.03$ the above algorithm agrees with the exact calculation within about 1% for scatterer thicknesses from 10^{-4} to 10^4 radiation lengths. Fig. 3.4 shows comparison with experimental data [10]. Calculations agree with experiment within errors.

For a mixture of N elements, the above equations need to be rewritten. For the near-Gaussian function (3.4), parameters become

$$< \theta^2 >= \sum_{i=1}^{N} \chi^2_{c,i}(\log \frac{\theta^2_{nuc,i}}{\chi^2_{a,i}} - C - 1),$$

$$< \theta^4 >= \sum_{i=1}^{N} \chi^2_{c,i}\theta^2_{nuc,i}.$$

If

$$D = \frac{< \theta^4 >}{2 < \theta^2 >^2} < 0.01,$$

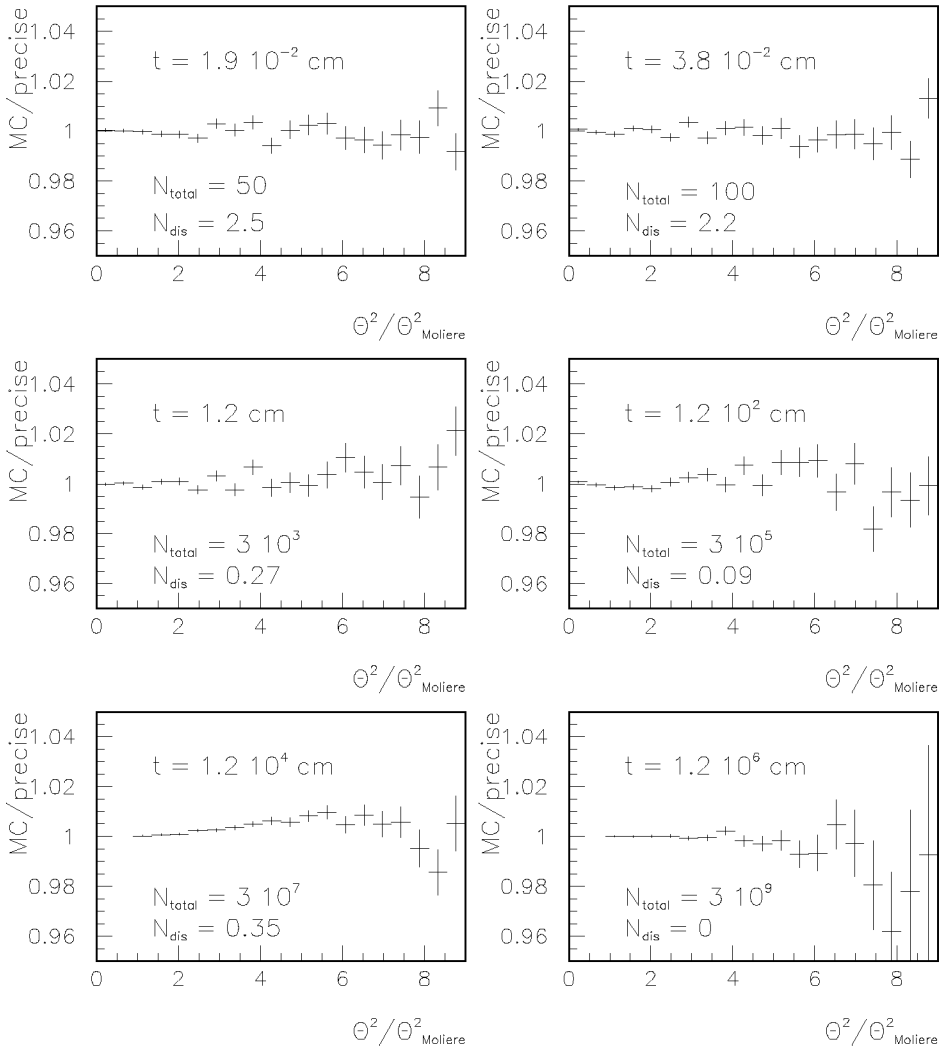

Figure 3.3: Angular distributions after lithium absorber.

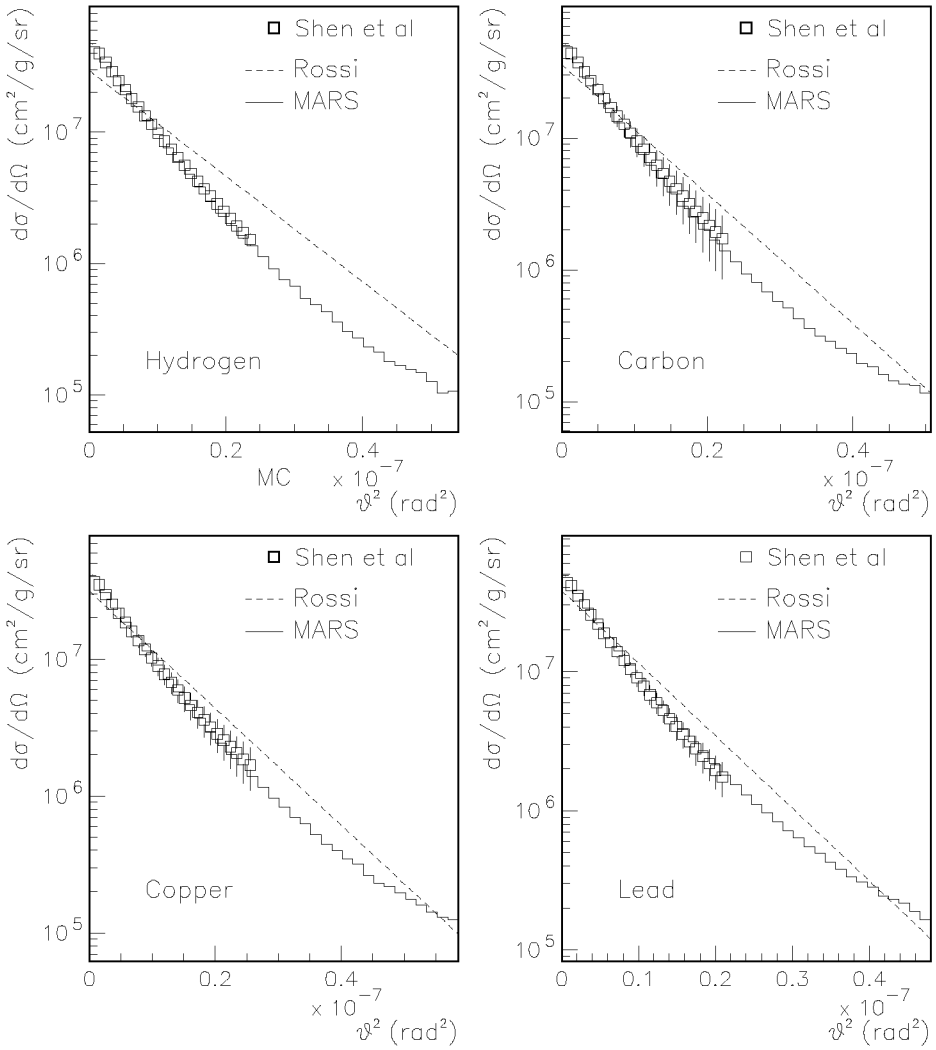

Figure 3.4: Angular distributions of 70 GeV protons after about 0.05 radiation length of different absorbers.

the angle is sampled from (3.4) with the above parameters, otherwise, one calculates threshold angle

$$\theta_0^2 = 8\delta x^2 X,$$

here x is calculated using the equation

$$x - \log x = \frac{1}{2}(\log(8\delta X) + Y/X - 1) \tag{3.15}$$

where

$$X = \sum_{i=1}^{N} \chi_{c,i}^2,$$

$$Y = -\sum_{i=1}^{N} \chi_{c,i}^2 \log(\chi_{a,i}^2).$$

Then $\theta_{max}^2 = min(\theta_0^2, \theta_{nuc-max}^2/10)$, where $\theta_{nuc-max}^2$ is chosen for the heaviest nuclei in mixture. For every element in the mixture, one calculates the number of discrete collisions and simulates corresponding angles.

Parameters of the "soft" distribution F_1 are calculated as

$$< \theta_1^2 >= \sum_{i=1}^{N} \chi_{c,i}^2 (\log(\theta_{max}^2/\chi_{a,i}^2) - 1),$$

where $z^2 = \frac{\theta^2}{\theta_1^2}$ and $D = \frac{\theta_{max}^2 X}{2<\theta_1^2>^2}$.

The total scattering angle is a vector sum of discrete and "soft" angles.

3.3 Code description

To simulate angular deflection on a step T, one calls

SUBROUTINE SAMCS(EKIN,T,AMASS,NELT,A,Z,W,TET)

INPUT PARAMETERS:
EKIN - kinetic energy in GeV,
T - step length in g/cm**2,
AMASS - mass of particle in GeV,
NELT - number of elements in mixture,
A(NELT) - array of atomic masses,
Z(NELT) - array of atomic numbers,
W(NELT) - array of relative weights.

OUTPUT PARAMETER:
TET - space angle in radian.

SAMCS calls CERNLIB routine/function RNDM, FLPSOR.

Bibliography

[1] N. V. Mokhov FERMILAB-FN-628 (1995);
N. V. Mokhov, O. E. Krivosheev FERMILAB-CONF-00-181;
http://www-ap.fnal.gov/MARS/

[2] N. V. Mokhov et al. FERMILAB-CONF-98-379, LA-UR-98-5716

[3] N. V. Mokhov and S. I. Striganov FERMILAB-CONF-98-035

[4] B. Rossi and K. Greisen Rev. Mod. Phys 13, p.240 (1941)

[5] G. Z. Molier, Z.Naturforsh 2a, p.133 (1947) Z.Naturforsh 3a, p.78 (1948)

[6] I. S. Baishev, N. V. Mokhov and S. I. Striganov Sov. J. Nucl. Phys. 42, p.745 (1985)

[7] S. I. Striganov Nucl. Phys. B (Proc. Suppl) 51A, p.172 (1996)

[8] P. Andreo and A. Brahme Rad. Res. 100, p.16 (1984)

[9] A. Van Ginneken Phys. Rev. D37, p.3292 (1988)

[10] G. Shen et al. Phys. Rev. D20, p.1584 (1979)